Version 2010-Aug-2

The Willouran Basic Province of South Australia: its relation to the Guibei Large Igneous Province in South China and the breakup of Rodinia

Xuan-Ce Wang[1, 2, 3]* Xian-Hua Li[1] Zheng-Xiang Li[2] Ying Liu[4] Yue-Heng Yang[1]

1. State Key Laboratory of Lithospheric Evolution, Institute of Geology and Geophysics, Chinese Academy of Sciences, P.O. Box 9825, Beijing 100029, China

2. The Institute for Geoscience Research, Department of Applied Geology, Curtin University, GPO Box U1987, Perth, WA 6845, Australia

3. School of Earth and Environment, the University of Western Australia, Crawley, WA 6009, Australia

4. Key Laboratory of Isotope Geochronology and Geochemistry, Guangzhou Institute of Geochemistry, Chinese Academy of Sciences, Guangzhou 510640, China

* Corresponding author. Present address: Department of Applied Geology, Curtin University of Technology, GPO Box U1987, Perth, WA 6845, Australia.
Phone: +61 8 9266 2453
Fax: +61 8 9266 3153
E-mail: X.Wang3@curtin.edu.au (X.C.Wang)

Abstract

The Willouran Basic Province in South-Central Australia and the Guibei large igneous province (LIP) in the South China Block are two of the most prominent Neoproterozoic LIPs related to the breakup of the supercontinent Rodinia. The Willouran Basic Province is dominated by tholeiitic mafic dykes (the Gairdner dykes), flood basalts (the Wooltana basalts), and mafic intrusions. The basaltic suites across a distance of more than 1000 km have similar immobile major element compositions, uniform tholeiitic OIB-type trace element distribution patterns, and identical Hf-Nd isotopic signatures. Geochemical analyses from this study imply that their generation may have involved both depleted and enriched mantle sources, similar to that of the Guibei LIP. The age distributions of the two LIPs are also comparable, peaking at ca. 825 Ma. This simultaneous flare-up of mafic magmatism in the two continents, including high-temperature lavas found in the South China Block, coincides with the starting up of widespread continental rifting in Rodinia. We thus speculate that the two LIPs could have been parts of a once contiguous LIP, which was dismembered during the breakup of Rodinia. This work thus provides additional support for the proposed South China-Australia connection in Rodinia.

Keywords: Neoproterozoic; Willouran Basic Province; Wooltana basalts; large igneous province; mantle plume; Australia, South China; Rodinia

1. Introduction

Large igneous provinces (LIPs) represent major magmatic events in Earth's history with areal extents > 0.1×10^6 km^2, igneous volumes > 0.1×10^6 km^3 and maximum lifespans of ~50 Myr that have intraplate tectonic settings or geochemical affinities (e.g., Coffin and Eldholm, 1992; Bryan and Ernst, 2008). They are generally thought to be produced by melting of the large spherical heads of new mantle plumes with diameters of 2000-2500 km (e.g., Richards et al., 1989; Campbell and Griffiths, 1990; Griffiths and Campbell, 1990; Campbell, 2007) although there are also non-plume models for the generation of such LIPs (e.g., King and Anderson, 1995). LIPs are commonly thought to be temporally and causally linked to the breakup of supercontinents, such as with the cases of the Parana, Karoo, and Deccan flood basalts accompanying the breakup of Pangea (e.g., Hill, 1991; Storey, 1995; Courtillot et al., 1999; Silver et al., 2006). In some instances, continental flood basalt provinces, the on-land members of LIPs, were dismembered by the breakup of supercontinents. For example, the Central Atlantic Magmatic Province was dismembered into four continental flood basalt provinces and is now preserved on four continents (North and South America, Africa and Europe; Marzoli et al., 1999; Nomade et al., 2007; Whiteside et al., 2007). Correlations of these dismembered LIPs are thus a critical source of information for reconstructing past supercontinents in Earth's history (e.g., Ernst et al., 2008; Li et al., 2008).

Despite the widely held consensus that continental rifting led to the fragmentation of the supercontinent Rodinia between 825 Ma and 750 Ma (Li et al., 2008 and

references therein), the mechanism of the breakup is still debated. Mantle plume activity has commonly been invoked as a cause of the breakup of Rodinia (e.g., Park et al., 1995; Li et al., 1999, 2002, 2003, 2005b, 2008; Ernst et al., 2008; Wang et al., 2007a, 2008, 2009; Li and Zhong, 2009), with evidence including radiating dyke swarms, high-temperature lavas, globally-synchronous anorogenic igneous activity, large-scale lithospheric doming and unroofing, and geochemical signatures similar to more recent plume magmatism.

South-Central Australia and the South China Block have some of the best-preserved Neoproterozoic magmatic records related to the breakup of Rodinia (e.g., Li et al., 2008 and references therein). Magmatic and rifting events, ca. 825-780 Ma, have been well documented on both continents, but their possible inter-relationship has not been rigourously tested. If the continents were indeed adjacent to each other in Rodinia as proposed by Li et al. (1995, 1999, 2003, 2008), the LIPs now preserved in both continents could be cogenetic. Alternatively, if South China was on the fringe of Rodinia (e.g., Zhao and Cawood, 1999), one would expect the development of arc magmatism in parts of South China. Indeed, the ca. 825-750 Ma magmatic events in South China have been alternatively interpreted by some to be of arc origin (e.g., Zhou et al., 2002, 2006; Wang et al., 2007b).

The Willouran Basic Province is the most important Neoproterozoic LIP in South-Central Australia (Fig. 1A and 1B), dominated by tholeiitic dykes, remnants of flood basalts, sills, and mafic-ultramafic intrusions (e.g., Crawford and Hilyard, 1990; Zhao et al., 1994; Wingate et al., 1998; Ernst et al., 2008). Pioneering geochemical,

91 petrographic, and stratigraphic work (e.g., Crawford and Hilyard, 1990; Hilyard, 1990;
92 Zhao et al., 1994) demonstrated that the Willouran Basic Province has features similar
93 to recent LIPs, such as the Columbia River, Parana, and Deccan continental flood
94 basalt provinces, but its petrogenesis and tectonic implications are not fully
95 understood.

96 In this paper, we present new major, trace element and Nd and Hf isotope data
97 for basalts from the Willouran Basic Province, and compare them with published data
98 for their South China equivalents. The results suggest that the two LIPs could be
99 correlated, thus lending further support for the proposed South China-Australia
100 connection in Rodinia.

101

102 **2. Geological setting and sampling**

103 The Adelaide Rift Complex consists of extensive, deeply subsided sedimentary
104 basins of Neoproterozoic to Early Cambrian (~830-515 Ma) age that overlie
105 Paleoproterozoic to Mesoproterozoic basement in southeastern Australia (e.g., Jenkins,
106 1990; Preiss, 1987, 2000). The Complex has a well preserved Neoproterozoic rift
107 succession, starting with the Willouran rift succession with associated basalts, through
108 clastic, glaciogenic and carbonate rocks until the rift-drift transition at the base of the
109 Tabley Hill Formation (ca. 650 Ma; Powell et al., 1994; Preiss, 2000; Kendall et al.,
110 2006) (Fig. 2).

111 The mafic igneous rocks comprise dykes, sills, and continental flood basalts that
112 spread across the Gawler Craton, the Adelaide Rift Complex, the Musgrave Block,

and the Amadeus Basin (Figs. 1A and 2). The volcanic rocks are preserved in normal stratigraphic sequence separated from the crystalline basement by thin basal coarse clastic rocks, and are conformably overlain by stromatolitic carbonates or calc-silicate sedimentary rocks (Fig. 2). They include the Wooltana Volcanic rocks, the Beda Volcanic rocks, the Cadlareena Volcanic rocks, the Wilangee Basalt, the Noranda Volcanic rocks, and basalts of the River Brougton beds. Together with dykes found in the Stuart Shelf (the Gairdner Dyke Swarm), its extension to the Musgrave Inlier and the Little Broken Hill Gabbro, this LIP has been called the Willouran Basic Province (Hilyard, 1990; Crawford and Hilyard, 1990; Ernst et al., 2008). The basaltic lavas within the Willouran Basic Province are hydrothermally altered (e.g., Crawford and Hilyard, 1990).

The Gairdner Dyke Swarm is recognised on aeromagnetic images as a NW-trending array of linear magnetic anomalies in the Gawler Craton and Stuart Shelf (Fig. 1A; Parker et al., 1987; Preiss, 2000). The dyke swarm has been equated with similarly trending Amata dykes in the Musgrave Inlier (Goode, 1970; Sun and Sheraton, 1996), indicating a total swarm length of ~1000 km (Fig. 1A). Geochemical analyses and stratigraphical comparisons suggest that the extrusive components (the Wooltana Volcanic rocks, the Beda Volcanic rocks, the Cadlareena Volcanic rocks, and the Wilangee Basalt) and the intrusive components (e.g., the Gairdner Dyke Swarm, the Amata dykes and the Little Broken Hill Gabbro) within the Willouran Basic Province were comagmatic (e.g., Mason et al., 1978; Crawford and Hilyard, 1990; Zhao and McCulloch, 1993; Zhao et al., 1994; Wingate et al., 1998). The age of

the intrusive magmatism is constrained by SHRIMP U-Pb zircon ages for the Gairdner Dyke Swarm (827 ± 6 Ma; Wingate et al., 1998), the Amata dykes (824 ± 4 Ma; Sun, S-s., unpublished data in Glikson et al., 1996) and the Little Broken Hill Gabbro (827 ± 9 Ma; Wingate et al., 1998) (Figs. 1A and 2).

The Wooltana Volcanics, at the base of the Adelaide Rift Complex, have long been a target for geochronological studies. However, low-temperature alteration of these mafic lavas hindered attempts to date this important igneous unit. An imprecise Rb-Sr isochron age of 830 ± 50 Ma was reported by Compston et al. (1996). The minimum eruptive age for the Wooltana Volcanics is constrained by the 802 ± 10 Ma U-Pb zircon age for the Rook Tuff in the upper Willouran sediments that overlies the Wooltana Volcanics (Fanning et al., 1986; Fig. 2). The maximum eruptive age for the Wooltana Volcanics is estimated at ca. 825 Ma based on the geochemical similarities and close stratigraphic relationships between the Gairdner Dyke Swarm and the Wooltana Volcanics (e.g., Zhao and McCulloch, 1993; Zhao et al., 1994; Preiss, 2000; Foden et al., 2002). Collectively, these results demonstrate that intrusive and extrusive rocks in the Willouran Basic Province are likely to have formed between ca. 830 and 800 Ma.

The Wooltana Volcanics in the northern part of the Adelaide Rift Complex is the most extensive outcropping unit. It consists of variably altered basalts, with minor dolerite-gabbro intrusions, rhyolite, rare andesite and interbedded sedimentary rocks (e.g., Fander, 1963; Crawford, 1963; Hilyard, 1990). The extensive sheet-like sub-aerial tholeiitic basalts have a total thickness of $\leq$ 2 km and generally lack pillows

157 or pyroclastic rocks (e.g., Hilyard, 1990). The basalts conformably overlie
158 calc-silicate sediments of the Arkaroola Subgroup and are disconformably overlain by
159 basal Terrensian or Sturtian sediments (Fig. 2; Preiss, 2000).

160 In this study, we sampled basalts at two major locations, Deport Creek and
161 Wooltana (Fig. 1). The Deport Creek Volcanics are exposed along Deport Creek near
162 the western edge of the Adelaide Rift Complex (sample sites AG04 to AG11), which
163 is adjacent to the Beda Volcanics over the Stuart Shelf (Fig. 1A). The Deport Creek
164 Volcanics range in colour from red, purplish to greenish and the basaltic flows are
165 generally quite amygdaloidal. In thin-section, the rocks are substantially altered and
166 vary from fine-grained, holocrystalline basalts with pilotaxitic texture, to hypalopilitic
167 varieties in which almost hair-like laths of plagioclase are scattered through what was
168 originally a glassy groundmass. Fresher basalts contain sericitised or albitised
169 plagioclase laths in a haematitic, chloritised matrix of pyroxene altered to actinolite or
170 tremolite, chlorite and epidote with introduced K-feldspar. There are amygdales that
171 contain calcite, quartz, chlorite, haematite, K-feldspar and albite. Basalt flows here are
172 range from 1-55 m thick, with separate flow pulses recognisable in coarser grained,
173 thick flows (e.g., Hilyard, 1990). The flows conformably overlie a dolomitic
174 sedimentary unit, and are disconformably overlain by the Emeroo Subgroup.

175 The other sampled location is the Wooltana Volcanics exposed near Wooltana in
176 the northeast corner of the Adelaide Rift Complex (Fig. 1A and 1C). The Wooltana
177 Volcanics comprise 610 m thick lavas associated with pyroclastic rocks (e.g.,
178 Crawford, 1963). The major part of the outcrop formed an almost north-south

179 volcanic belt (Figs. 1A and 1C). No pillow lavas have been found and most of the
180 volcanic rocks are subaerial, but the presence of interbedded thin, shallow-water
181 sedimentary rocks suggests that at least some flows were erupted sub aqueously (e.g.,
182 Hilyard, 1990; Crawford, 1963). The volcanic rocks are overlain disconformably by
183 Torrensian sediments (ca. 780-720 Ma; Preiss, 2000) or unconformably overlain by
184 the Sturtian glacial sequences (Fig. 1C and 2). The volcanic rocks are dominated by
185 basaltic lavas, with subsidiary porphyritic rhyolite and some andesite.

186 Sampling at Wooltana was carried out along three creek beds (Fig. 1C). The main
187 rock types sampled were amygdaloidal basalts, olivine dolerite, and ophitic olivine
188 dolerite. The colours of the rocks range through purple, reddish-brown, to grey or
189 dark-grey, sometimes with a faint greenish tinge. In thin-section, the rocks vary from
190 fine-grained, holocrystalline basalts with pilotaxitic texture, to basalts with a
191 hyalopilitic texture or locally with an ophitic structure. The dominant phenocrysts are
192 similar in all samples and included olivine, plagioclase, and pyroxene. Petrographic
193 examination suggests an order of crystallization of the original minerals as spinel,
194 olivine, feldspar, and then pyroxene (e.g., Mawson, 1926; this study). The rocks were
195 subjected to various degrees of alteration. For example, original glass has in some
196 cases been completely converted to opaque dusty aggregates and pyroxene has been
197 converted to secondary actinolite, microscopic particles of epidote, chlorite and
198 possibly serpentine. The alteration products of olivine are serpentine and opaques
199 minerals (magnetite and haematite). In summary, the main alteration products are
200 serpentine, tremolite, chlorite and epidote with introduced K-feldspar (e.g., Mawson,

1926; Fander, 1963; Crawford and Hilyard, 1990; this study). Secondary calcite occurs in veins and cavities.

3. Analytical techniques

After petrographic examination, the least-altered samples were selected for whole-rock geochemical analyses at the Guangzhou Institute of Geochemistry, Chinese Academy of Sciences. The samples were crushed to 1-0.5 cm chips and leached alternately with 0.4 and 0.2mol/L HCl and 0.6 and 0.3mol/L HNO_3 to remove surface contamination and to eliminate calcareous alteration. After leaching, the rock chips were ground to <200 mesh using a tungsten carbide mill. Major element oxides were analysed using a Rigaku RIX 2000 X-ray fluorescence spectrometer (XRF) on fused glass beads. Calibration lines used in quantification were produced by bi-variant regression of data from 36 reference materials encompassing a wide range of silicate compositions (Li et al., 2005a). The uncertainty for major elements is <5%.

Trace elements were analysed using an inductively coupled plasma mass spectrometer (Perkin-Elmer Sciex ELAN 6000 ICP-MS) following the analytical procedures described by Li et al. (2000). About 40 mg sample powders were dissolved in high-pressure Teflon bombs using a HF+HNO_3 mixture. An internal standard solution containing the single element Rh was used to monitor signal drift during analysis. A set of standard rocks including GSR-1, GSR-2, GSR-3, W-2, G-2 and SY-4 were used for calibrating element concentrations in the measured samples. The uncertainty for most trace elements analysed is <2%. Reproducibility, based on

223 replicate digestion of samples, is better than 10 % for most analyses.

224 Nd isotopic compositions were determined using a Micromass Isoprobe
225 multi-collector ICP-MS (MC-ICP-MS) at the Guangzhou Institute of Geochemistry,
226 using analytical procedures described by Li et al. (2004a). Nd fractions were
227 separated by passing through cation columns followed by HDEHP columns, and the
228 aqueous sample solution was taken up in 2% HNO_3 and introduced into the
229 MC-ICP-MS using a Meinhard glass nebuliser with an uptake rate of 0.1 ml/min. The
230 inlet system was cleaned for 5 min between analyses using high purity 5% HNO_3
231 followed by a blank solution of 2% HNO_3. Measured $^{143}Nd/^{144}Nd$ ratios were
232 normalized to $^{146}Nd/^{144}Nd = 0.7219$, and the reported $^{143}Nd/^{144}Nd$ ratios were further
233 adjusted relative to the Shin Etsu JNdi-1 standard of 0.512115, corresponding to the
234 La Jolla standard of 0.511860 (Tanaka et al., 2000).

235 For Hf isotopic analyses, ca. 100 mg rock powders were homogeneously mixed
236 with 200 mg $Li_2B_4O_7$. The mixtures were digested for 15 min at 1200 ℃ in Pt–Au
237 crucibles, then dissolved in 2M HCl. Hf fractions were separated following a
238 modified single-column separation procedure through ion exchanges using an
239 Eichrom® Ln-Specresin (Li et al., 2007a). Hf isotopic ratios were analysed using a
240 Finnigan Neptune MC-ICPMS at the State Key Laboratory of Lithospheric Evolution,
241 Institute of Geology and Geophysics, Chinese Academy of Sciences, Beijing.
242 Measured $^{176}Hf/^{177}Hf$ ratios were normalized to $^{179}Hf/^{177}Hf = 0.7325$, and the reported
243 $^{176}Hf/^{177}Hf$ ratios were further adjusted relative to the JMC-475 standard ($^{176}Hf/^{177}Hf$
244 = 0.282160). During the course of this study, international standard rocks BHVO-2

and JB-1 yielded $^{176}Hf/^{177}Hf$ = 0.283099 ± 6 (2σ, n = 7) and 0.282974 ± 7 (2σ, n = 7), respectively, which are in good agreement with the results reported by Kleinhanns et al. (2002).

4 Results

4.1 Major and trace element compositions

Based on petrographic examination and loss on ignition (LOI) values, twenty of the least altered samples were selected for major and trace element analysis. Compositions of the basalts from Wooltana Volcanics and Deport Creek Volcanics are shown in Table 1. With the exception of one andesitic sample, the Wooltana basalts have relatively uniform SiO_2 (50 – 54 wt.%, volatile-free), TiO_2 (1.4 – 2.3 wt.%), Al_2O_3 (12 – 16 wt.%), and FeOt (10 – 14 wt.%) contents, but highly variable MgO (6 – 12 wt.%), CaO (0.2 – 6.4 wt.%), K_2O (1 – 6 wt.%) and Na_2O (0.4 – 4.3 wt.%) contents (Fig. 3 and Table 1). The Deport Creek Volcanics (DCV) display similar major element compositions, but are relatively enriched in MgO (10 – 14 wt.%) and K_2O (>4 wt.%) compared with the Wooltana Volcanics. As shown in Figure 3, samples from Deport Creek Volcanics, Wooltana Volcanics, Beda Volcanics and Bitter Springs Volcanics display general correlations between SiO_2, FeO^T, TiO_2, MgO and Na_2O contents and FeO*/MgO ratios. The Al_2O_3, CaO and K_2O do not appear to correlate with FeO^T/MgO ratios (Figs. 3C, 3G and 3H). On the Zr/TiO_2-Nb/Y diagram (Fig. 4), the two basalt suites have similar Nb/Y ratios ranging from 0.20 to 0.49 (mostly between 0.20 and 0.26), both plotting in the sub-alkaline field. They also have typical tholeiitic affinities with FeO^T and TiO_2 increasing with elevated FeO^T/MgO

ratios (Figs. 3B and 3E).

The Wooltana and Deport Creek basalts display slight enrichment in light rare earth element (LREE) with $(La/Yb)_N$ = 1.3-3.0 (mostly between 2.1-2.9, where subscript N denotes chondrite normalization) and fractionated heavy REE (HREE) patterns [$(Sm/Yb)_N$ = 1.5-2.0] (Figs. 5A and 5B). The Wooltana and Deport Creek basalts have similar "humped" incompatible trace elemental distribution patterns (Fig. 6), which are characterized by variable enrichment in all the incompatible trace elements except P, Nb, and Ta. The immobile trace element compositions of the extrusive components within the Willouran Basic Province remarkably resemble those of the coeval mafic dykes (Figs. 5-6). They show geochemical characteristics similar to typical mantle plume-derived continental flood basalts (e.g., the Deccan Traps) and tholeiitic OIB (e.g., Hawaii) (Fig. 6).

4.2 Nd and Hf isotopes

Nd and Hf isotope data for 16 relatively fresh samples are presented in Table 2. The samples have variable Nd isotopic compositions with $^{143}Nd/^{144}Nd$ = 0.51254-0.51271 and εNd_{825} = +0.7 to +6.5. The highest positive initial Nd isotopic value (+6.5) is from sample AG15 (Wooltana Volcanics exposed near Wooltana; Fig.1C). Its REE pattern is characterized by greater enrichment in LREE (La-Eu) but similar HREE (Gd-Lu) contents to other samples (Fig. 5B). Three of the samples (AG11, AG18 and AG20) display relatively low εNd_{825} values (+1.3, +0.7, and 1.1). These samples also show anomalous REE patterns with relatively depleted LREE, but

similar HREE contents compared with the others (Fig. 5). The remaining Wooltana Volcanics (WV) and Deport Creek Volcanics (DCV) have relatively uniform Nd isotopic compositions, similar to the Gairdner Dyke Swarm (GDS; Zhao et al., 1994), with εNd_{825} of +2 to +4 (Fig. 7). The Deport Creek Volcanics and Wooltana Volcanics have fairly uniform measured Hf isotopic ratios with $^{176}Hf/^{177}Hf$ = 0.28272 – 0.28280, corresponding to initial Hf isotopic compositions of εHf_{825} = +6.7 to +9.5. The Hf isotopes correlate well with Al_2O_3/TiO_2, Yb/Lu, and Lu/Hf ratios (Fig. 8).

In summary, the Deport Creek Volcanics and Wooltana Volcanics show similar geochemical, Hf-Nd isotopic and petrographic features suggesting that the two basalt suites may have a common origin. This is consistent with previous conclusions that Deport Creek Volcanics are equivalent to the Wooltana Volcanics (e.g., Crawford, 1963; Crawford and Hilyard, 1990; Hilyard, 1990).

5. Petrogenetic interpretations and discussion

5.1 Effects of secondary alteration on the geochemical and isotopic systems

All samples used in this study experienced no metamorphism, but they show a large range of LOI values (up to 6.2 wt.%) and abundant secondary minerals, indicating varying degrees of alteration.

Bulk compositions of the analysed samples are shown on an A-CN-K diagram in Fig. 9 (Nesbitt and Young, 1984, 1989). The least-altered samples plot close to the feldspar join (the line connecting the plagioclase and K-feldspar compositions), implying that feldspars are the most abundant aluminous minerals of the samples. In

312 Figure 9, most Wooltana samples (WV) plot between idealized plagioclase and
313 phyllosilicates (illite and muscovite), suggesting that the alteration involved the
314 conversion of plagioclase to phyllosilicates. The composition of the Deport Creek
315 samples (DCV) approaches the A (Al_2O_3)-K (K_2O) boundary in the A-CN-K diagram
316 (Fig. 9), indicating that almost all of the Ca and Na has been leached from the rocks.
317 The trend towards the K apex represents K-metasomatism (e.g., Nesbitt and Young,
318 1984). Most Deport Creek samples (DCV) and a few of the Wooltana samples plot on
319 the right of the line representing the limitation of weathering (dashed line "3" in Fig.
320 9), implying the introduction of K-feldspar.

321 Effects of alteration on major element compositions are determined by CIW
322 diagrams [CIW = Al_2O_3/ (Al_2O_3 + CaO + Na_2O), molecular ratio; Harnois, 1988] (Fig.
323 10). The strongly negative correlation of CaO-CIW (Fig. 10C) indicates that the
324 alteration resulted in CaO depletion. The positive correlation of K_2O-CIW (Fig. 10E)
325 reflects K-metasomatism (e.g., Crawford and Hilyard, 1990). A slight negative
326 correlation of Na_2O-CIW at > 50 CIW (Fig. 10F) suggests that Na has been leached
327 out from plagioclase due to its breakdown. A slight positive correlation between MgO
328 and CIW implies that the alteration caused some enrichment in MgO. At CIW <50,
329 SiO_2, Al_2O_3, FeO^T, and P_2O_5 shows no correlation with CIW (Fig. 10A, 10B, 10D,
330 and 10H), implying essential immobility. Figure 10 thus indicates that (1) fresh
331 samples should contain CaO >7 wt.%, SiO_2 = 47 – 52 wt.%, 1 wt.% <Na_2O <3 wt.%,
332 K_2O <3 wt.%, Al_2O_3 = 12 – 14 wt.%, FeO^T = 10 – 13 wt.%, and MgO = 6 – 12 wt.%;
333 (2) The Deport Creek samples underwent significant alteration and nearly all their

major elements have been disturbed.

Bivariate plots of Zr against selected trace elements can be used for evaluating the motilities of such elements during alteration (e.g., Polat et al., 2002). Figure 11 shows that REE (Nd and Yb), high field strength elements (HFSEs) Nb and Ti, and Lu and Y are tightly correlated with Zr, indicating that these elements were essentially immobile during metamorphism and alteration. However, these elements in some samples (AG11, AG15, AG20, AG29, and AG35) display different behaviours (Figs. 5 and 11), implying that the elements in these samples may be mobile. Alkaline elements (such as Rb and Cs), alkaline earth elements (such as Ca, Sr, and Ba), and transition metal elements (Sc, Cr, Co, Ni, and Mn) are scattered (figures not shown), implying varying degrees of mobility.

The Sm-Nd isotopic systems in most samples have not been significantly disturbed by alteration, as indicated by the lack of correlation of εNd(t) with CIW (not shown) and the relatively uniform εNd(t) values (Fig. 7). In a few exceptions (samples AG11, AG15, AG18, and AG20) the Sm-Nd isotopic system may have been disturbed by alteration processes.

5.2. Nature of the mantle sources for the Willouran Basic Province

The basaltic suites, spread across a distance of more than 1000 km including the Gairdner Dyke Swarm (Zhao et al., 1994; Foden et al., 2002), the Wooltana Volcanics (Crawford and Hilyard, 1990; Zhao et al., 1994; Foden et al., 2002; this study), the Deport Creek Volcanics (this study), the Bitter Springs Volcanics (Zhao et al., 1994),

and the Beda Volcanics (Foden et al., 2002), have identical average major element compositions: ~51 wt.% SiO_2, ~1.6 wt.% TiO_2, 14 wt.% Al_2O_3 and ~12 wt.% FeO^T (volatile-free). Together with their uniform trace element distribution patterns (Figs. 5-6) and similar Nd isotopic compositions (Fig. 7), the basaltic suites were most likely derived from a common mantle source at similar melting conditions, and underwent insignificant crustal contamination. Considering the complex Archean to Proterozoic crustal history of South-Central Australia, different crustal domains would have had distinct influences on the geochemical and Nd isotopic features of the basaltic units. Therefore, the similar geochemical and isotopic characteristics from different basaltic suites rule out the possibility of significant crustal contamination.

The nature of the mantle source can be constrained by Figure 8 because these ratios are insensitive to low-pressure magma differentiation, but are highly influenced by the source region. The correlations shown in Figure 8 may reflect the heterogeneity of the mantle source or binary mixing of depleted and enriched end-member melts. The enriched end-member melts are characterized by εHf_{825} = +6 to +7, εNd_{825} = +2 to +3, $Al_2O_3/TiO_2 \approx 12.7$, Lu/Hf ≈ 0.18, Sm/Yb ≈ 1.1, Hf/Yb ≈ 0.86, and Zr/Y ≈3.3. The depleted end-member melts are similar to the typical tholeiitic OIB-type melts (e.g., Hawaiian picrite; Norman and Garcia, 1999) with εHf_{825} = +9 to +11, εNd_{825} = +4 to +6, $Al_2O_3/TiO_2 \approx 6$, Lu/Hf ≈ 0.08, Sm/Yb ≈ 2.47, Hf/Yb ≈ 1.86, and Zr/Y ≈ 5.58. The corresponding Nd isotopes are estimated according to Hf isotopes based on the terrestrial array of $\varepsilon Hf(t) = 1.4\varepsilon Nd(t) + 3$ (Vervoort et al., 1999). These estimated values are consistent with the bimodal Nd isotopic distribution: one peak at about +3,

and the other peak at +5 (Fig. 7A).

One possible mantle source for such enriched end-member melts is sub-continental lithospheric mantle. However, sub-continental lithospheric mantle is too cold and refractory to melt at the scale required to form flood basalts (Gallagher and Hawkesworth, 1992). Alternatively, the enriched end-member melts could be derived mainly from recycled oceanic crust because the end-member melts have Hf-Nd isotope compositions ($\varepsilon Nd = +2$ and $\varepsilon Hf = +6$ to $+7$) resembling that of 1 Ga recycled oceanic crust ($\varepsilon Nd = +2.5$ and $\varepsilon Hf = +6$; Stracke et al., 2003). Therefore, we prefer that the enriched end-member melts were derived mainly from recycled oceanic crust. A rising plume head would also have entrained lower mantle so that the melts are mixtures of materials from the boundary layer plume source and entrained lower mantle (Campbell and Griffiths, 1990; Campbell, 2007). Therefore, the enriched end-member melts may also reflect contributions from FOZO or the lower mantle (Hart et al., 1992).

5.3. Parts of a dismembered large igneous province associated with the breakup of Rodinia?

Although it has long been recognized that the ca. 825 Ma Willouran Basic Province in Australia was likely the product of a mantle plume (e.g., Crawford and Hilyard, 1990; Hilyard, 1990; Zhao et al., 1994), the position of the plume head remains an open question. Zhao et al. (1994) proposed that the plume head was located to the south-east of the Willouran Basic Province.

On the other hand, there is considerable evidence for the presence of a ca. 825 Ma plume-head beneath South China. This includes the widespread occurrence of anorogenic magmatism with rock types ranging from granite to mafic–ultramafic dykes and sills (implying the presence of mafic underplating and a large heat source), large-scale syn-magmatic doming, and the development of ca. 820 Ma continental rift systems (Li et al., 2008 and references therein), and importantly, the recent identification of the 823 ± 6 Ma high-temperature Yiyang komatiitic basalts (Wang et al., 2007a). The primary melt of the Yiyang komatiitic basalts has a typical high Mg composition and implies a melt temperature of >1500°C.

Z.X. Li et al. (1999, 2003, 2008) suggested that the South China Block could have been sited between Australia and Laurentia within Rodinia based on tectonic-stratigraphy studies. Therefore, if both the presence of the a ca. 825 Ma plume head beneath South China and Z.X. Li et al.'s (1995, 2008) reconstruction are correct, the remnants of LIPs in South-Central Australia and north and northwestern South China Block would have been causally and spatially linked.

Figure 12A plots all available magmatic ages from the South China Block (see Appendix Table 1). The age distribution of Neoproterozoic magmatism in the South China block matches well with that of South-Central Australia (Fig. 12C). Figure 12B and 12D shows that mafic magmatism in South China, represented by the Guibei LIP (e.g., Li et al., 2008; Ernst et al., 2008), mainly occurred between 830 and 810 Ma, which is similar to that of the Willouran Basic Province (highlighted as the heavy grey band in Fig. 12A-D). The two LIPs have the same peak age of ca. 823 Ma, which is

422 identical to the 823 Ma age for the high-temperature Yiyang komatiitic basalts in
423 central South China (Wang et al., 2007a). Furthermore, the flood basalts from the two
424 regions share similar trace element distribution patterns (Fig. 13), highly incompatible
425 trace element ratios (Fig. 14). Together with previous tectonostratigraphic studies (Li
426 et al., 1995, 1999, 2008), these similarities suggest that (1) the Adelaide Rift Complex
427 and the Bikou-Hannan Rift may have been part of a triple-junction rifting system with
428 the Adelaide Rift Complex being a failed rift; and (2) the synchronous LIPs in South
429 China Block and in South-Central Australia represent the dismembered parts of a
430 single LIP that formed during the breakup of the supercontinent Rodinia (Fig. 15).
431 Figure 15B illustrates our revised geodynamic model for the generation of the
432 830-810 Ma LIP, called the Willouran-Guibei LIP that spread across South China and
433 southern Australia. A mantle plume is suggested to have impinged at the base of the
434 continental lithosphere beneath the Yangtze craton at ca. 830 Ma. The Yangtze
435 cratonic keel would have deflected the plume head to two major pre-existing
436 lithospheric weak zones, one being between the Yangtze and Australian cratons, the
437 other being the Sibao orogen between the Yangtze and Cathaysia cratons, both leading
438 to the intrusion or eruption of LIP magmatism and continental rifting (Fig. 15A and B).
439 The initial phase of the LIP event may have occurred at ca. 830 Ma and peaked at ca.
440 825 Ma, followed by continental rifting.
441 If this interpretation is correct, the Willouran-Guibei LIP would have served as a
442 major source for Neoproterozoic sediments in both Australia and South China due to
443 large scale crustal doming, and the hypothesis could thus be further tested by

444 comparing the Nd isotopes in the rift successions of the two continents. In the
445 Adelaide Rift Complex, a “positive Nd isotope shift” has been identified in the late
446 Neoproterozoic sedimentary sequences, interpreted as reflecting the erosion of
447 continental flood basalts (Barovich and Foden, 2000). A similar Nd isotope signature
448 has also been identified in Neoproterozoic rifting successions in South China,
449 featuring an increase in εNd(t) value from -7 to +1 (e.g., Li and McCulloch, 1996).
450 These data thus support the single LIP model.
451 Recognition of a ca. 825 Ma dismembered LIP throughout the northwestern
452 margin of the South China Block and South-Central Australia has important
453 implications for mineral deposits, including Ni-Cu-PGEs and V-Ti mineralization.
454 The majority of world-class magmatic Ni-Cu-PGE sulfide deposits are related to flood
455 basalts of mantle plume origin (i.e., Noril’sk-Talnakh and Duluth) and large layered
456 mafic-ultramafic complexes (i.e., Bushveld and Great Dyke of Zimbabwe) (Naldrett,
457 1997). In addition, the world’s third largest Ni-Cu sulfide deposit at Jinchuan dated at
458 ca. 830 Ma (Li et al., 2005b), the ca. 825 Ma Gaojiacun Ni-Cu-PGE sulfide deposit in
459 the western South China Block (Zhu et al., 2007) and the synchronous Fe-V-Ti
460 deposits at Hannan near the northwestern margin of the South China Block (Su, 2004)
461 may also be related to this LIP. However, major deposits of this age have not been
462 reported in Australia.
463 We note that Zhou and coworkers have proposed an arc model for the
464 Neoproterozoic igneous rocks in South China (e.g., Zhou et al., 2002, 2006). Their
465 main evidence for this stems from the depletions of Nb, Ta and Ti found in some of

the igneous rocks, mostly in granitoids (Zhou et al., 2002). However, it has been argued that arc-like geochemical signatures in continental felsic rocks should not be used as diagnostic indicators for subduction settings because such signatures are often inherited from the source rocks (e.g., Wang et al., 2009; Li et al., 2006). The subduction model is also inconsistent with a number of other geological, geochemical and petrological observations in the region such as a regional structural trend in western South China Block that is at high angle to that predicted by the arc model, the large distances between many of the plutons and the then continental margins, the close temporal and spatial links between plutonism and continental rifting, and extremely H_2O-poor but high-T melt conditions (e.g., Li et al., 2006, 2007b, 2009; Wang and Li, 2003; Wang et al., 2007a, 2008, 2009, 2010).

6. Conclusions

A combination of new geochemical analyses of basaltic rocks in the Willouran Basic Province of South-Central Australia with previous results and a comparison with similar rocks in South China enable us to reach the following conclusions:

(1) Similar geochemical and isotopic characteristics from basaltic suites in the >1000 km Willouran Basic Province were most likely derived from a common mantle source at similar melting conditions, and underwent insignificant crustal contamination. Our work suggests that the basalts were likely derived from mixing of depleted and enriched end-member melts. The enriched end-member melts may be derived mainly from recycled oceanic crust or entrained lower

mantle materials.

(2) The close similarities both in their ages and their geochemical and isotopic characteristics suggest that the Willouran Basic Province and the Guibei LIP in South China were likely integral parts of a single LIP that was dismembered during the breakup of the supercontinent Rodinia.

Acknowledgements

We thank Professors Ian Campbell and Richard Ernst, an anonymous reviewer and editor Andrew Kerr for their constructive and helpful reviews. We are grateful to D.A.D. Evans and T. Raub for assisting with field sampling, X.R. Liang, X.L. Tu, G.Q. Hu, J. Li, and W. Zeng with assistance in geochemical analyses and Professor Simon Wilde for comments. This work was supported by the NSFC (grants 40721063 and 40773007) and an ARC Discovery Project grant (DP0770228). This is TIGeR (The Institute of Geoscience Research) publication #228.

502 References

503 Barovich, K.M. and Foden, J., 2000. A Neoproterozoic flood basalt province in
504 southern-central Australia: geochemical and Nd isotope evidence from basin
505 fill. Precambrian Research 100, 213-234.

506 Bryan, S.E. and Ernst, R.E., 2008. Revised definition of Large Igneous Provinces
507 (LIPs). Earth-Science Reviews 86, 175-202.

508 Campbell, I.H., 2007. Testing the plume theory. Chemical Geology 241, 153-176.

509 Campbell, I.H., Griffiths, R.W., 1990. Implications of mantle plume structure for the
510 evolution of flood basalts. Earth and Planetary Science Letters 99, 79-93.

511 Compston, W., Crawford, A.C., Bofinger, V.M., 1996. A radiometric estimate of the
512 duration of sedimentation in the Adelaide Geosyncline. South Australia.
513 Journal of the Geological Society of Australia 13, 229-276.

514 Coffin, M. F., Eldholm, O., 1992. Volcanism and continental break-up: A global
515 compilation of large igneous provinces. In: B.C. Storey, T. Alabaster, and R. J.
516 Pankhurst (Editors), Magmatism and the Causes of Continental Break-Up.
517 Geological Society, London, Special Publications 68, 21-34.

518 Courtillot, V., Jaupart, C., Manighetti, I., Tapponnier, P., and Besse, J., 1999. On the
519 causal links between flood basalts and continental breakup. Earth and
520 Planetary Science Letters 166, 177–195.

521 Crawford, A.J., Hilyard, D., 1990. Geochemistry of late Proterozoic tholeiitic flood
522 basalts, Adelaide Geosyncline, South Australia. In: Jago, J.B. and Moore, P.S.
523 (Eds.), The evolution of a Late Precambrian-Early Palaeozoic rift complex:

524 The Adelaide Geosyncline. Geological Society of Australia Special
525 Publication 16, 49-67.
526 Crawford. R., 1963. The Wooltana volcanic belt, South Australia. Transactions of the
527 royal society of South Australia 87, 123-154.
528 Ernst, R.E., Wingate, M.T.D., Buchan, K.L., Li, Z.X., 2008. Global record of
529 1600–700 Ma Large Igneous Provinces (LIPs): Implications for the
530 reconstruction of the proposed Nuna (Columbia) and Rodinia supercontinents.
531 Precambrian Research 160, 159–178.
532 Fabris, A., Constable, S., Conor, C., Woodhouse, A., Hore, S., Fanning, M., 2005.
533 Age, origin, emplacement and mineral potential of the Oodla Wirra Volcanics,
534 Nackara Arc, central Flinders Ranges. MESA Journal 37, 44–52.
535 Fanning, C.M., Ludwig, K.R., Forbes, B.G., Preiss, W.V., 1986. Single and multiple
536 grain U–Pb zircon analyses for the early Adelaidean Rook Tuff, Willouran
537 Ranges, South Australia. Abstracts/Geological Society of Australia 15, 71-72.
538 Fander, H.W., 1963. The Wooltana lavas. Transactions of the royal society of South
539 Australia 87, 155-158.
540 Foden, J., Song, S.H., Tuner, S., Elburg, M., Smith, P.B., Steldt, B.V., Penglis, B.V.,
541 2002. Geochemical evolution of lithospheric mantle beneath S.E. South
542 Australia. Chemical Geology 182, 663-695.
543 Gallagher, K., Hawkesworth, C., 1992. Dehydration melting and the generation of
544 continental flood basalts. Nature 258, 57–59.
545

546 Glikson, A.Y., Stewart, A.J., Ballhaus, C.G., Clarke, G.L., Feeken, E.H.J., Leven,
547 J.H., Sheraton, J.W., Sun, S.S., 1996. Geology of the western Musgrave Block,
548 central Australia with particular reference to the mafic-ultramafic Giles
549 Complex. Australian Geological Survey Organisation Bulletin 239, 206 pp.
550 Goode, A.D.T., 1970. The petrology and structure of the Kalka and Ewarara layered
551 basic intrusions, Giles Complex, central Australia. Ph.D thesis, University of
552 Adelaide.
553 Griffiths, R.W., Campbell, I.H., 1990. Stirring and structure in mantle starting plumes.
554 Earth and Planetary Science Letters 99, 66–78.
555 Harnois, L., 1988. The CIW index: A new chemical index of weathering. Sedimentary
556 Geology 55, 319-322.
557 Hart, S.R., Hauri, E.H., Oschmann, L.A., Whitehead, J.A., 1992. Mantle plume and
558 entrainment: Isotopic Evidence. Science 256, 517-520.
559 Hill, R.I., 1991. Starting plumes and continental break-up. Earth and Planetary
560 Science Letters 104, 398-416.
561 Hilyard, D., 1990. Willouran Basic Province: Stratigraphy of Late Proterozoic flood
562 basalts, Adelaide Geosyncline, South Australia. In: Jago, J.B. and Moore, P.S.
563 (Eds.), The evolution of a Late Precambrian-Early Palaeozoic rift complex:
564 The Adelaide Geosyncline. Geological Society of Australia Special
565 Publication 16, 34-48.
566 Jenkins, R., 1990. The Adelaide Fold Belt: tectonic reappraisal. Geological Society of
567 Australia Special Publication 16, 396–420.

568 Kendall, B., Creaser, R.A., Selby, D., 2006. Re-Os geochronology of postglacial black
569 shales in Australia: Constraints on the timing of "Sturtian" glaciation. Geology
570 34, 729-732.
571 King, S. D., Anderson, D.L., 1995. An alternative mechanism of flood basalt
572 formation. Earth and Planetary Science Letters 136, 269-279.
573 Kleinhanns, I.C., Kreissig, K., Kamber, B.S., Meisel, T., Nagler, T.F., Kramers, J.D.,
574 2002. Combined Chemical Separation of Lu, Hf, Sm, Nd, and REEs from a
575 Single Rock Digest: Precise and Accurate Isotope Determinations of Lu-Hf
576 and Sm-Nd Using Multicollector-ICPMS. Analytical Chemistry 74, 67-73.
577 Li, X.H., Liu, Y., Yang, Y.H., Chen, F.K., Tu, X.L., Qi, C.S., 2007a. Rapid separation
578 of Lu-Hf and Sm-Nd from a single rock dissolution and precise measurement
579 of Hf-Nd isotopic ratios for national rock standards. Acta Petrologica Sinica
580 23, 221-226 (in Chinese with English abstract).
581 Li, X.H., Li, Z.X., Sinclair, J.A., Li, W.X., Carter, G., 2007b. Reply to the comment by
582 Zhou et al. on: “Revisiting the “Yanbian Terrane”: Implications for
583 Neoproterozoic tectonic evolution of the western Yangtze Block, South China”.
584 Precambrian Research, 155, 318-323.
585 Li, X.H., Li, Z.X., Sinclair, J.A., Li, W.X., Carter, G., 2006. Revisiting the “Yanbian
586 Terrane”: implications for Neoproterozoic tectonic evolution of the western
587 Yangtze Block, South China. Precambrian Research 151, 14-30.
588 Li, X.H., Qi, C.S., Liu, Y., Liang, X.R., Tu, X.L., Xie, L.W., Yang, Y.H., 2005a.
589 Petrogenesis of the Neoproterozoic bimodal volcanic rocks along the western

590 margin of the Yangtze Block: new constraints from Hf isotopes and Fe/Mn
591 ratios. Chinese Science Bulletin 50, 2481–2486.
592 Li, X.H., Su, L., Chung, S.L., Li, Z.X., Liu, Y., Song, B., Liu D.Y., 2005b. Formation
593 of the Jinchuan ultramafic intrusion and the world's third largest Ni-Cu sulfide
594 deposit: Associated with the ~825 Ma south China mantle plume?
595 Geochemistry, Geophysics, Geosystems 6, Q11004,
596 doi:10.1029/2005GC001006.
597 Li, X.H., Liu, D., Sun, M.I.N., Li, W.-X., Liang, X.-R., and Liu, Y., 2004a, Precise
598 Sm-Nd and U-Pb isotopic dating of the supergiant Shizhuyuan polymetallic
599 deposit and its host granite, SE China. Geological Magazine 141, 225-231.
600 Li, X.H., Li, Z.X., Zhou, H., Liu, Y., and Kinny, P.D., 2002. U-Pb zircon
601 geochronology, geochemistry and Nd isotopic study of Neoproterozoic
602 bimodal volcanic rocks in the Kangdian Rift of South China: implications for
603 the initial rifting of Rodinia. Precambrian Research 113, 135-154.
604 Li X.H., Sun M., Wei G.J., Liu Y., Lee C.Y., Malpas J.G., 2000. Geochemical and
605 Sm-Nd isotopic study of amphibolites in the Cathaysia Block, SE China:
606 evidence for extremely depleted mantle in the Paleoproterozoic. Precambrian
607 Research 102, 251-262.
608 Li, X.H., McCulloch, M.T., 1996. Secular variation in the Nd isotopic composition of
609 Neoproterozoic sediments from the southern margin of the Yangtze Block:
610 evidence for a Proterozoic continental collision in southeast China.
611 Precambrian Research 76, 67-76.
612 Li, Z.X., Li, X.H. and Wang, X.C., 2009. The South China piece in the Rodinian

puzzle: A reply to the comment by Munteanu and Wilson. Precambrian Research 171, 77-79.

Li, Z.X., Zhong, S., 2009. Supercontinent-superplume coupling, true polar wander and plume mobility: Plate dominance in whole-mantle tectonics. Physics of the Earth and Planetary Interiors 176, 143-156.

Li, Z.X., Bogdanova, S.V., Collins, A.S., Davidson, A., De Waele, B., Ernst, R.E., Fitzsimons, I.C.W., Fuck, R.A., Gladkochub, D.P., Jacobs, J., Karlstrom, K.E., Lu, S., Natapov, L.M., Pease, V., Pisarevsky, S.A., Thrane, K. and Vernikovsky, V., 2008. Assembly, configuration, and break-up history of Rodinia: A synthesis. Precambrian Research 160, 179-210.

Li, Z.X., Li, X.H., Kinny, P.D., Wang, J., Zhang, S. and Zhou, H., 2003. Geochronology of Neoproterozoic syn-rift magmatism in the Yangtze Craton, South China and correlations with other continents: evidence for a mantle superplume that broke up Rodinia. Precambrian Research 122, 85-109.

Li, Z.X., Li, X.H., Kinny, P.D., Wang, J., 1999. The breakup of Rodinia: did it start with a mantle plume beneath South China? Earth and Planetary Science Letters 173, 171-181.

Li, Z.X., Zhang, L., Powell, C.M., 1995. South China in Rodinia: part of the missing link between Australia-East Antarctica and Laurentia. Geology 23, 407-410.

Ling, W., Gao, S., Zhang, B., Li, H., Liu, Y. Cheng, J., 2003. Neoproterozoic tectonic evolution of the northwestern Yangtze craton, South China: implications for amalgamation and break-up of the Rodinia Supercontinent. Precambrian

635 Research 122, 111-140.
636 Ludwig, K.R., 2001. Users manual for Isoplot/Ex rev. 2.49. Berkeley Geochronology
637 Centre Special Publication. No. 1a, 56 pp.
638 Marzoli, A., Renne, P., Piccirillo, E., Ernesto, M., Bellieni, G., and De Min, A., 1999.
639 Extensive 200-million-year-old continental flood basalts of the Central
640 Atlantic Magmatic Province. Science 284, 616–618.
641 Mason, M.G., Thomas, B.P., Tonkin, D.G., 1978. Regional stratigraphy of Beda
642 Volcanics, Backy Point Beds and Pandurra Formation on the Stuart Shelf,
643 South Australia. Quarterly Geological nots, Geological survey of South
644 Australia 66, 2-9.
645 Mawson. D., 1926. The Wooltana Basic Igneous Belt. Transactions of the royal
646 society of South Australia 47, 376-387.
647 Melluso, L., Mahoney, J.J. and Dallai, L., 2006. Mantle sources and crustal input as
648 recorded in high-Mg Deccan Traps basalts of Gujarat (India). Lithos 89, 259
649 -274.
650 Naldrett, A. J., 1997. Key factors in the genesis of Noril'sk, Subdury, Jinchuan,
651 Voisey's Bay and other world-class Ni-Cu-PGE deposits: Implications for
652 exploration. Australian Journal of Earth Sciences 44, 283–316.
653 Nesbitt H. W. and Young G. M., 1989. Formation and diagenesis of weathering
654 profiles. Journal of Geology 97, 129-147.
655 Nesbitt, H. W. and Young, G. M., 1984. Prediction of some weathering trends of
656 plutonic and volcanic rocks based on thermodynamic and kinetic

considerations. Geochimica et Cosmochimica Acta 48, 1523-1534.

Nomade, S., Knight, K.B., Beutel, E., Renne, P.R., Verati, C. Féraud, G., Marzoli, A., Youbi, N., Bertrand, H., 2007. Chronology of the Central Atlantic Magmatic Province: Implications for the Central Atlantic rifting processes and the Triassic–Jurassic biotic crisis. Palaeogeography, Palaeoclimatology, Palaeoecology 244, 326-344.

Norman, M.D. and Garcia, M.O., 1999. Primitive magmas and source characteristics of the Hawaiian plume: petrology and geochemistry of shield picrites. Earth and Planetary Science Letters 168, 27-44.

Park, J.K., Buchan, K.L. and Harlan, S.S., 1995. A proposed giant radiating dyke swarm fragmented by the separation of Laurentia and Australia based on paleomagnetism of ca.780 Ma mafic intrusions in western North America. Earth and Planetary Science Letters 132, 129-139.

Parker, A.J., Rickwood, P.C., Baillie, P.W., Boyd, D.M., Freeman, M.J., McCenaghan, M.P., Murray, C.G., Myers, J.P., and Pietsch, B.A.,1987. Mafic dyke swarms of Australia, in: Mafic Dyke Swarms, H.C. Halls and W.F. Fahrig, eds., Geological Society of Australia Special Publication 16, 129-148.

Polat, A., Hofmann, A.W., Rosing, M.T., 2002. Boninite-like volcanic rocks in the 3.7-3.8 Ga Isua greenstone belt, West Greenland: geochemical evidence for intra-oceanic subduction zone processes in the early Earth. Chemical Geology 184, 231-254.

Powell, C.M., Preiss, W.V., Gatehouse, C.G., Krapez, B., Li, Z.X., 1994. South Australian record of a Rodinian epicontinental basin and its mid-Neoproterozoic breakup (~700 Ma) to form the Palaeo-Pacific Ocean. Tectonophysics 237, 113-140.

682 Preiss, W.V., Fanning, C.M., Szpunar. M., Burtt, A.C., 2008. Age and tectonic
683 significance of the Mount Crawford Granite Gneiss and a related intrusive in
684 the Oakbank Inlier, Mount Lofty Ranges. MESA Journal 49, 38-49.
685 Preiss, W.V., 2000. The Adelaide Geosyncline of South Australia and its significance
686 in Neoproterozoic continental reconstruction. Precambrian Research 100,
687 21-63.
688 Preiss, W.V., 1987. The Adelaide Geosyncline–Late Proterozoic stratigraphy,
689 sedimentation, paleontology, and tectonics. Australian Geological Survey
690 Organisation Bulletin 53, 438.
691 Richards, M.A., Duncan, R.A., Courtillot, V.E., 1989. Flood basalts and hotspot tracks:
692 plume heads and tails. Science 246, 103-107.
693 Silver, P.G., Behn, M.D., Kelley, K., Schmitz, M., Savage, B., 2006. Understanding
694 cratonic flood basalts. Earth and Planetary Science Letters 245, 190-201.
695 Storey, B.C., 1995. The role of mantle plumes in continental breakup: case histories
696 from Gondwanaland. Nature, 377, 302-308.
697 Stracke, A., Bizimis, M., Salters, V.J.M., 2003. Recycling oceanic crust: Quantitative
698 constraints. Geochemistry, Geophysics, Geosystems 4, 8003, doi: 10.1029
699 /2001GC000223.
700 Su, L., 2004. Studies of Neoproterozoic mafic and ultramafic intrusions in
701 western-central China and their constraints on breakup of Rodinia supercontinent,
702 Ph.D. thesis, 107 pp., Northwest Univ., Xi’an, China.
703 Sun, S.S., McDonough, W.F., 1989. Chemical and isotopic systematics of oceanic

basalts: implications for mantle composition and processes. In: A.D. Saunders and M.J. Norry (Editors), Magmatism in the Ocean Basins. Geological Society, London, Special Publications 42, 313-345 pp.

Sun, S.S., Sheraton, J.W., 1996. Geochemical and isotopic evolution. In: A.Y. Glikson et al. (Editors), Geology of the Western Musgrave Block, Central Australia, with Particular Reference to the Mafic–Ultramafic Giles Complex. Australian Geological Survey Organisation (AGSO) Bulletin 239, pp. 135-143.

Tanaka, T., Togashi, S., Kamioka, H., Amakawa, H., Kagami, H., Hamamoto, T., Yuhara, M., Orihashi, Y., Yoneda, S., Shimizu, H., Kunimaru, T., Takahashi, K., Yanagi, T., Nakano, T., Fujimaki, H., Shinjo, R., Asahara, Y., Tanimizu, M., Dragusanu, C., 2000. JNdi-1: a neodymium isotopic reference in consistency with La Jolla neodymium. Chemical Geology 168, 279-281.

Vervoort, J.D., Patchett, P.J., Blichert-Toft, J., Albarede, F., 1999. Relationships between Lu-Hf and Sm-Nd isotopic systems in the global sedimentary system. Earth and Planetary Science Letters 168, 79-99.

Wang, J. and Li, Z.-X., 2003. History of Neoproterozoic rift basins in South China: implications for Rodinia break-up. Precambrian Research 122, 141-158.

Wang, Q., Wyman, D.A., Li, Z.X., Bao, Z.W., Zhao, Z.H., Wang, Y.X., Jian, P., Yang, Y.H., Chen, L.L., 2010. Petrology, geochronology and geochemistry of ca. 780 Ma A-type granites in South China: Petrogenesis and implications for crustal growth during the breakup of the supercontinent Rodinia. Precambrian

Research 178, 185-208.

Wang, X.C., Li, X.H., Li, W.X., Li, Z.X, 2009. Variable involvements of mantle plumes in the genesis of mid-Neoproterozoic basaltic rocks in South China: A review. Gondwana Research 15, 381-395.

Wang, X.C., Li, X.H., Li, W.X., Li, Z.X., Liu, Y., Yang, Y.H., Liang, X., R., Tu, X.L., 2008. The Bikou basalts in northwestern Yangtze Block, South China: Remains of 820-810 Ma continental flood basalts? Geological Society of American Bulletin 120, 1478-1492.

Wang, X.C., Li, X.H., Li, W.X., Li, Z.X., 2007a. Ca. 825 Ma komatiitic basalts in South China: First evidence for >1500°C mantle melts by a Rodinian mantle plume. Geology 35, 1103–1106.

Wang, X.-L., Zhou, J.-C., Griffin, W.L., Wang, R.-C., Qiu, J.-S., O'Reilly, S.Y., Xu, X., Liu, X.-M., Zhang, G.-L., 2007b. Detrital zircon geochronology of Precambrian basement sequences in the Jiangnan orogen: Dating the assembly of the Yangtze and Cathaysia Blocks. Precambrian Research 159, 117-131.

Wingate, M.T.D., Campbell, I.H., Compston, W., Gibson, G.M., 1998. Ion microprobe U-Pb ages for Neoproterozoic basaltic magmatism in south-central Australia and implications for the breakup of Rodinia. Precambrian Research 87, 135-159.

Winchester, J.A., Floyd, P.A., 1976. Geochemical magma type discrimination: application to altered and metamorphosed basic igneous rocks. Earth and Planetary Science Letters 28, 459-469.

748 Whiteside, J.H., Olsen, P.E. Kent, D.V. Fowell S.J., Et-Touhami, M. 2007.
749 Synchrony between the Central Atlantic magmatic province and the
750 Triassic-Jurassic mass-extinction event? Palaeogeography, Palaeoclimatology,
751 Palaeoecology 244, 345-367.
752 Zhao, J.-X., McCulloch, M.T., 1993. Sm-Nd mineral isochron ages of Late
753 Proterozoic dyke swarms in Australia: evidence for two distinctive events of
754 mafic magmatism and crustal extension. Chemical Geology 109, 341-354.
755 Zhao, J.-X., McCulloch, M.T., Korsch, R.J., 1994. Characterisation of a plume-related
756 ~800 Ma magmatic event and its implications for basin formation in
757 central-southern Australia. Earth and Planetary Science Letters 121, 349-367.
758 Zhao, G.C., Cawood, P.A., 1999. Tectonothermal evolution of the Mayuan assemblage
759 in the Cathaysia Block: Implications for neoproterozoic collision- related
760 assembly of the South China craton. American Journal of Science, 299,
761 309-339.
762 Zhou, M.F., Ma, Y.X., Yan, D.P., Xia, X.P., Zhao, J.H., Sun, M., 2006. The Yanbian
763 Terrane (Southern Sichuan Province, SW China): a late proterozoic arc
764 assemblage in the western margin of the Yangtze Block. Precambrian
765 Research 144, 19-38.
766 Zhou, M., Kennedy, A.K., Sun, M., Malpas, J., Lesher, C.M., 2002. Neoproterozoic
767 arc-related mafic intrusions along the northern margin of South China;
768 implications for the accretion of Rodinia. Journal of Geology 110, 611-618.
769 Zhu, W.-G., Zhong, H., Li, X.-H., Liu, B.-G., Deng, H.-L., Qin, Y., 2007. ^{40}Ar-^{39}Ar

770 age, geochemistry and Sr-Nd-Pb isotopes of the Neoproterozoic Lengshuiqing
771 Cu-Ni sulfide-bearing mafic-ultramafic complex, SW China. Precambrian
772 Research 155, 98-124.

Figure caption

Fig. 1 (A) Simplified geological map of the Neoproterozoic Willouran Basic Province showing sample locations, compiled after Wingate et al. (1998) and Crawford and Hilyard (1990). Inset (B) shows the regional extent of the Willouran Basic Province (after Crawford and Hilyard, 1990, Wingate et al., 1998, and Ernst et al., 2008). (C) Detail sampling locations for the Wooltana Volcanics in the northern Adelaide Rift Complex. The main basaltic units include: DCV = Deport Creek Volcanics; WV = Wooltana Volcanics; BV = Beda Volcanics; BCV = Boucaut Volcanics; BSV = Bitter Springs Volcanics; Ca = Cadlareena Volcanics; GDS = Gairdner Dyke Swarm, NV =Noranda Volcanics. Source of quoted ages: [1] Wingate et al. (1998); [2] Glikson et al. (1996); [3] Preiss et al. (2008); [4] Fabris et al., 2005; [5] Fanning M. unpublished data, cited in Preiss, 2000.

Fig. 2 Schematic composite stratigraphy for Neoproterozoic rocks in the Adelaide Rift Complex and adjacent platforms (after Wingate et al., 1998). No thicknesses are implied and the entire sequence is not present at any single locality. Source of quoted ages: [1] Kendall et al. (2006); [2] Fanning M. unpublished data, cited in Preiss (2000); [3] Fanning et al. (1986); [4] Fabris et al. (2005); [5] Preiss et al. (2008); [6] Wingate et al. (1998).

Fig. 3 Plots of major elements vs. FeO^T/MgO ratios for the extrusive components (BSV, BV, DCV, and WV) and intrusive components (GDS) within the Willouran

795 Basic Province. Data for GDS are from Crawford and Hilyard (1990), Zhao et al.
796 (1994), and Foden et al. (2002); BSV from Zhao et al. (1994); BV from Foden et al.
797 (2002). Open circles represent the data for the Wooltana Volcanics from Crawford and
798 Hilyard (1990) and Foden et al. (2002). The other data (WV and DCV) are from this
799 study. Abbreviations for rocks units are as in Figure 1.
800
801 **Fig. 4** $Zr/TiO_2 \times 0.0001$ vs. Nb/Y diagram distinguishing sub-alkaline and alkaline
802 basalts (Winchester and Floyd, 1976).
803
804 **Fig. 5** Chondrite-normalized REE diagrams for samples of the Deport Creek
805 Volcanics, Wooltana Volcanics, Bitter Spring Volcanics, and Beda Volcanics. Shaded
806 area outlines data range for the Gairdner Dyke Swarm and the Amata dykes (after
807 Zhao et al., 1994). See text for discussion. The data for Bitter Springes Volcanics and
808 Beda Volcanics are from Zhao et al. (1994) and Foden et al. (2002), respectively. The
809 chondrite-normalized values and N-MORB, E-MORB and typical alkaline OIB data
810 are from Sun and McDonough (1989).
811
812 **Fig. 6** Primitive mantle-normalized incompatible trace element spidergrams for (A)
813 Bitter Spring Volcanics (BSV), (B) Deport Creek Volcanics (DCV); and (C) Wooltana
814 Volcanics (WV). Data for the Bitter Spring Volcanics are from Zhao et al. (1994). All
815 other data are from this study. Shaded area outlines data from the Gairdner Dyke
816 Swarm (after Zhao et al., 1994). The Hawaiian picrite is the average of samples with

MgO varying from 14 to 18 wt.% (N = 11; Norman and Garcia, 1999). Data for the Deccan high-Ti picrite are from Melluso et al. (2006). The primitive mantle-normalized values, N-MORB, E-MORB, and typical alkaline OIB data are from Sun and McDonough (1989).

Fig. 7 Histograms for Nd distributions of (**A)** the Gairdner Dyke Swarm (GDS; Zhao et al., 1994; Foden et al., 2002); (B) the Deport Creek Volcanics (DCV; this study); (C) the Wooltana Volcanics (WV; Foden et al., 2002; this study); (D) Willouran Basic Province combined data.

Fig. 8 Plots of (A) Lu/Hf; (B) Hf/Yb, (C) Al_2O_3/TiO_2; (D) Yb/Lu vs. εHf_{825}. These trends suggest that the generation of the Wooltana Volcanics (WV) and Deport Creek Volcanics (DCV) involved at least two end-member melts. See text for discussion. (E) εHf_{825} versus εNd_{825} plot of the Wooltana and Deport Creek basalts compared to 'terrestrial array' ($\varepsilon Hf = 1.36\varepsilon Nd + 2.95$; Vervoort et al., 1999).

Fig. 9 Samples from the Willouran Basic Province plotted on an A-CN-K diagram (Nesbitt and Young, 1989). Abbreviations are: $A = Al_2O_3$; $CN = CaO+Na_2O$; $K = K_2O$; Ka = Kaolin; Gib = gibbsite; Sm = smectite; P1 = plagioclase; and Ks = K-feldspar; IL = illite; Mu= Muscovite. Line "1" represents the predicted weathering trend. Line "2" indicates a metasomatic trend. Basalts from the Willouran Basic Province defined a trend (line 3) that lies removed from the predicted weathering trend and the decrease

in slope of the line “3” indicates K-metasomatism has occurred. Dashed line “4” is the limit of weathering. Data sources: Wooltana Volcanics (WV, Crawford and Hilyard, 1990; Foden et al., 2002; this study); Deport Creek Volcanics (DCV, this study); Bitter Spring Volcanics (BSV, Zhao et al. (1994); Gairdner Dyke Swarm (GDS; Zhao et al., 1994; Foden et al., 2002).

Fig. 10 Selected major elements vs. CIW variation diagrams highlighting the effects of alteration on major elements. CIW = Al_2O_3/ (Al_2O_3 + CaO + Na_2O), molecular ratio (Harnois, 1988). For abbreviations and data source see the caption of Figure 9

Fig. 11 Variation diagrams of selected elements vs. Zr. Data sources: WV and DCV – this study; GDS and BSV – Zhao et al. (1994). Abbreviations as in Fig. 9.

Fig. 12 Age distribution of igneous rocks in South China and South Australia between 850 and 750 Ma: (A) all igneous rocks in South China; (B) mafic rocks only in South China; (C) all igneous rocks in Australia; (D) mafic rocks only in South-Central Australia; (E) weighted mean age for the 830-800 Ma magmatism (the Guibei LIP) in South China; (F) weighted mean age for the Willouran Basic Province of South Australia. The geochronological data are listed in Appendix 1. In (D) and (E), the grey band is 1% uncertainties relative to the weighted mean ages. Plots were generated using ISOPLOT (Ludwig, 2001).

Fig. 13 REE (A) and trace element (B) distribution patterns, comparing the Willouran Basic Province (WBP) with the Tiechuanshan (TCS)-Bikou flood basalts. The average of lower and upper Bikou group basalts are shown in (B) as L-BK and U-BK, respectively. Data for the Bikou Group and the Tiechuanshan basalts are from Wang et al. (2008) and Ling et al. (2003), respectively. Data for the Willouran Basic Province are from Zhao et al. (1994) and this study.

Fig. 14 Comparative plots of (A) Nb/Y vs. Zr/Y; (B) Hf/Yb vs. Lu/Hf; (C) Nb/Y vs. Lu/Hf; (D) Zr/Hf vs. Nb/Ta; (E) TiO2 vs. Lu/Hf; (F) Zr/Y VS. Lu/Hf; (G) Nb/la-Nb/Th-Th/La; and (H) Lu/Hf-Sm/Nd-Nb/Y for the Bikou-Tiechuanshan continental flood basalts and the Willouran Basic Province. Data for the Bikou-Tiechuanshan continental flood basalts are from Wang et al. (2008) and Ling et al. (2003); data for the Willouran Basic Province are from Zhao et al. (1994) and this study. These plots imply that the basalts from the two basaltic suites most likely derived from a common mantle source and involved both enriched and depleted end-members. Two ternary diagrams (G-H) further demonstrate that mantle heterogeneity may play an important role in generating the geochemical diversity of these basalts.

Fig. 15 (A) the distribution of the proposed single large igneous province in the Rodinia reconstruction of Li et al. (2008). (B) Cartoon diagram showing the proposed model for the genesis of the large igneous province including the Nanhua, Kangdian, Bikou-Hannan, and Adelaide rift systems. The dark grey field shows the possible

distribution of the large igneous province.

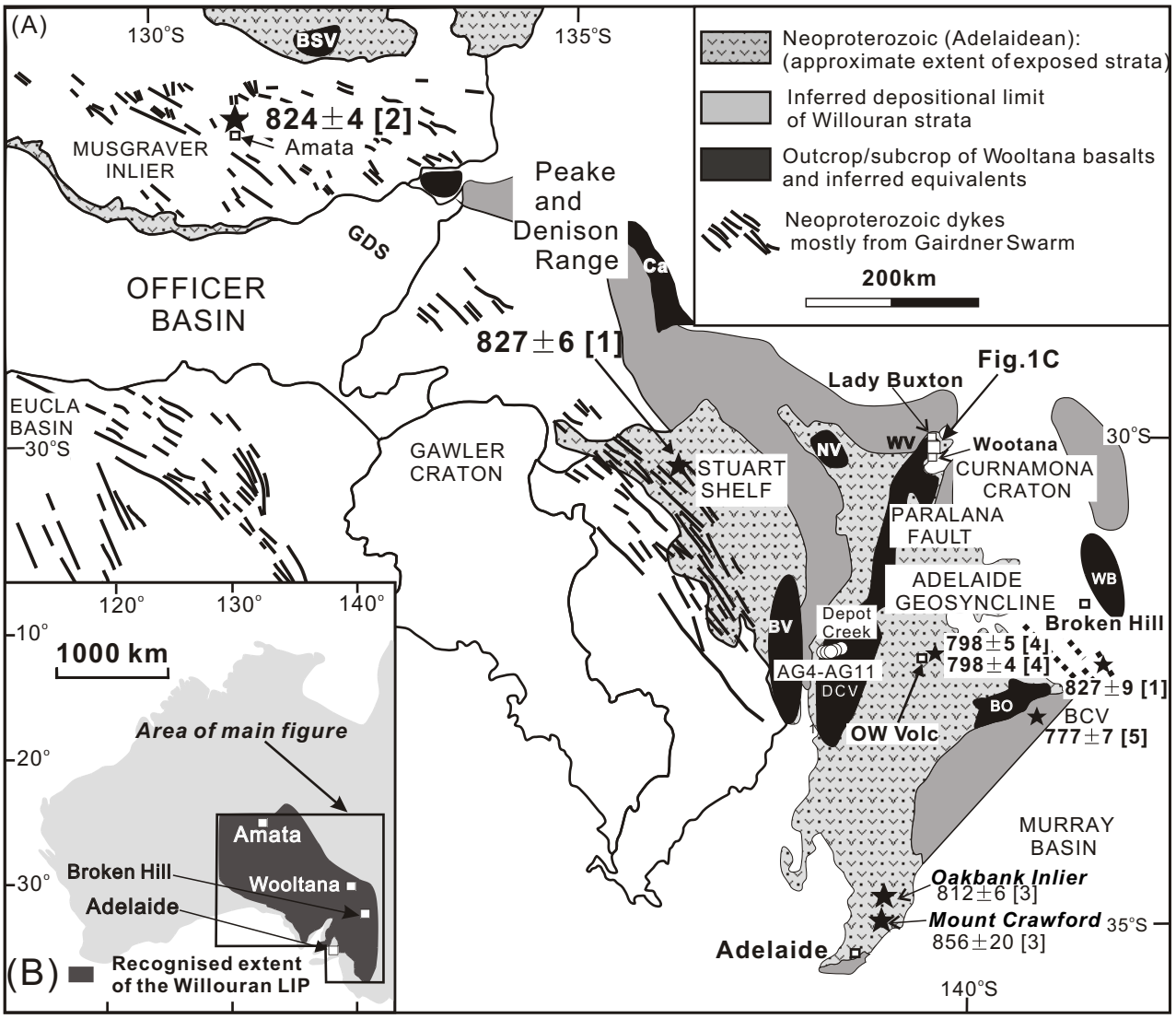
(A)
130°S
135°S
BSV
824±4 [2]
Amata
MUSGRAVER INLIER
GDS
Peake and Denison Range
Ca
OFFICER BASIN
827±6 [1]
Neoproterozoic (Adelaidean): (approximate extent of exposed strata)
Inferred depositional limit of Willouran strata
Outcrop/subcrop of Wooltana basalts and inferred equivalents
Neoproterozoic dykes mostly from Gairdner Swarm
200km
Fig.1C
Lady Buxton
EUCLA BASIN
30°S
GAWLER CRATON
NV
WV
Wootana
CURNAMONA CRATON
STUART SHELF
PARALANA FAULT
ADELAIDE GEOSYNCLINE
WB
BV
Depot Creek
Broken Hill
798±5 [4]
798±4 [4]
827±9 [1]
AG4-AG11
DCV
BO
BCV
777±7 [5]
OW Volc
MURRAY BASIN
Oakbank Inlier
812±6 [3]
Mount Crawford
856±20 [3]
35°S
Adelaide
140°S
120°
130°
140°
10°
20°
30°
1000 km
Area of main figure
Amata
Broken Hill
Wooltana
Adelaide
(B)
Recognised extent of the Willouran LIP

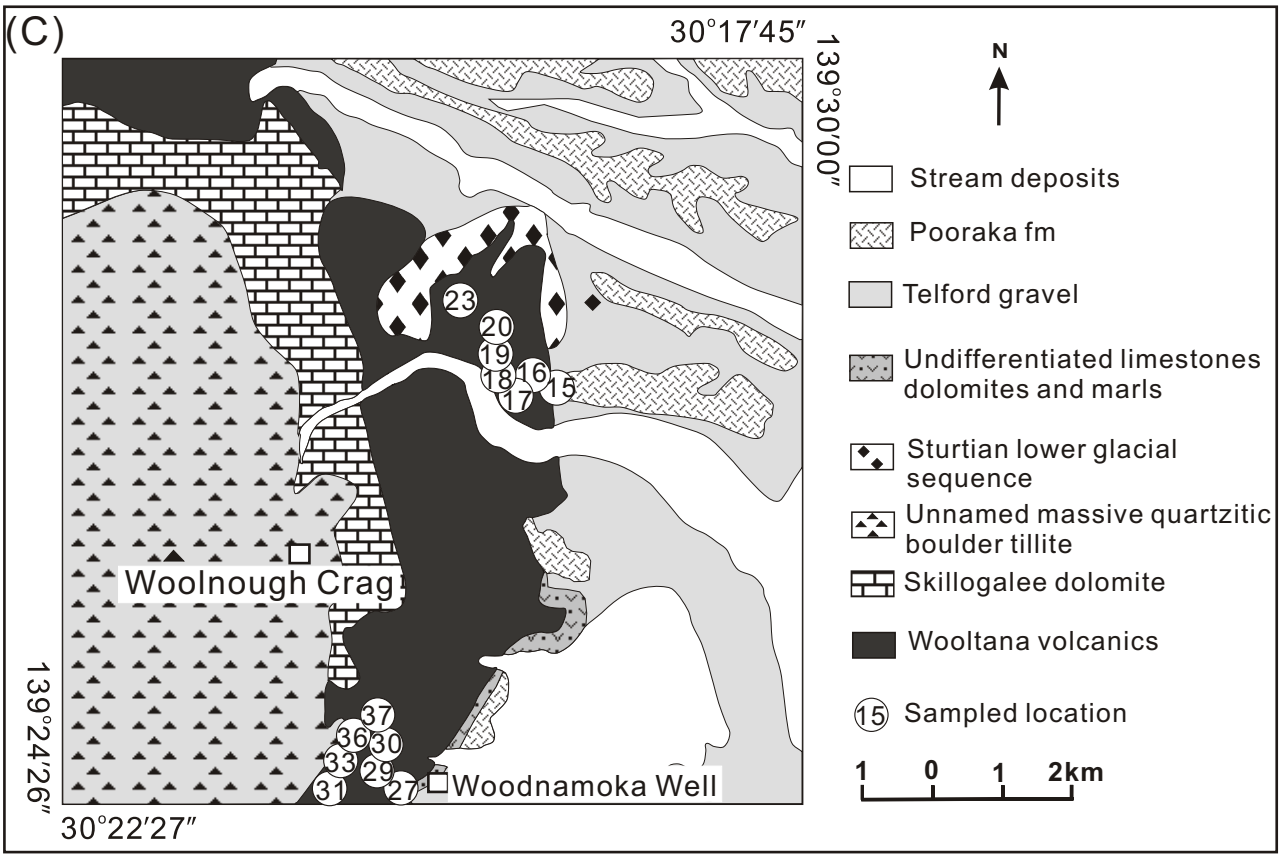
(C)
30°17′45″
139°30′00″
N
Stream deposits
Pooraka fm
Telford gravel
Undifferentiated limestones dolomites and marls
Sturtian lower glacial sequence
Unnamed massive quartzitic boulder tillite
Skillogalee dolomite
Wooltana volcanics
15 Sampled location
1 0 1 2km
Woolnough Crag
Woodnamoka Well
23
20
19
18
16
17
15
37
36
30
33
29
31
27
139°24′26″
30°22′27″

Fig. 1

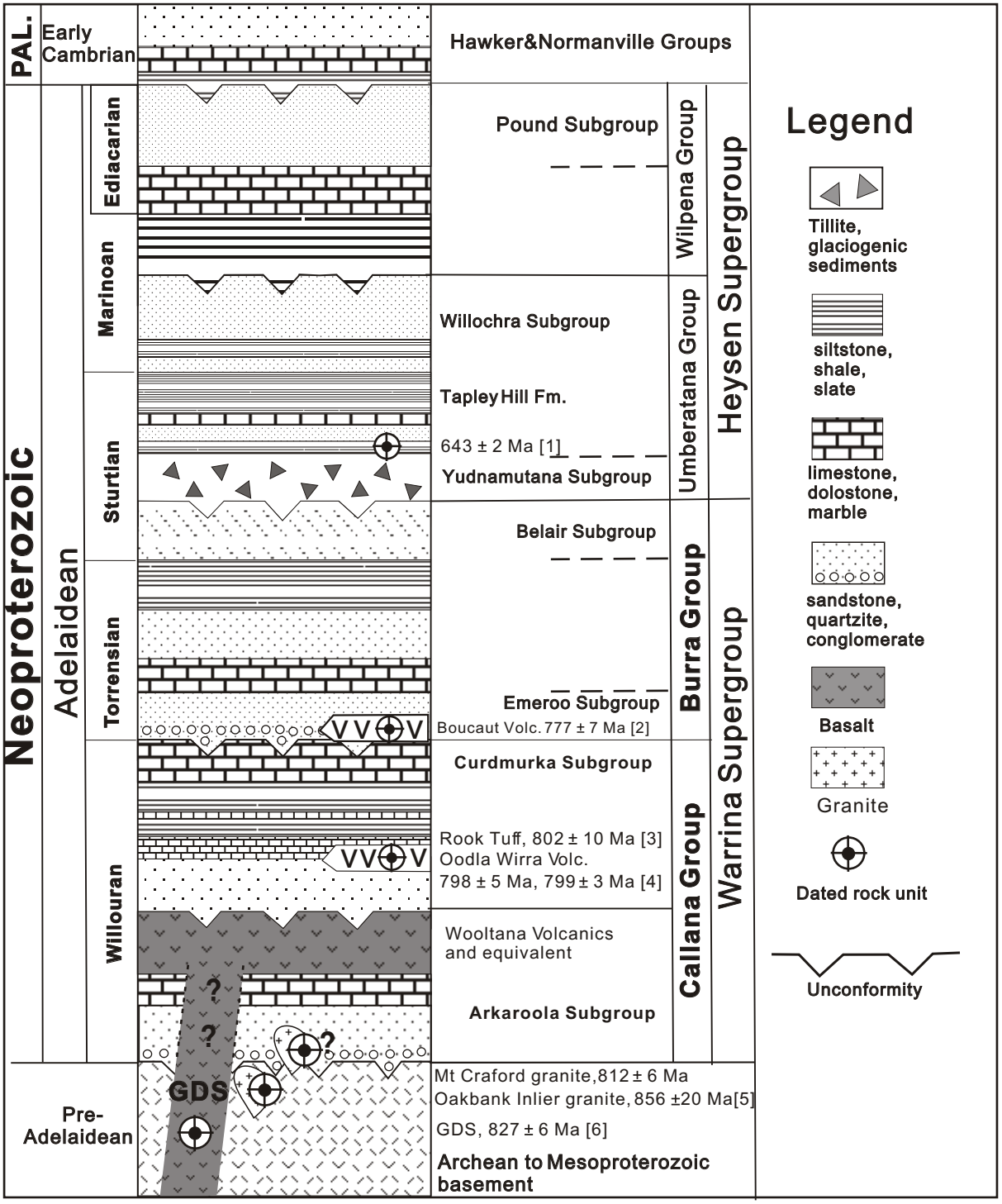
PAL.
Early Cambrian
Neoproterozoic
Adelaidean
Ediacarian
Marinoan
Sturtian
Torrensian
Willouran
Pre-Adelaidean
GDS
Hawker&Normanville Groups
Pound Subgroup
Wilpena Group
Willochra Subgroup
Tapley Hill Fm.
643 ± 2 Ma [1]
Yudnamutana Subgroup
Umberatana Group
Heysen Supergroup
Belair Subgroup
Emeroo Subgroup
Boucaut Volc. 777 ± 7 Ma [2]
Burra Group
Curdmurka Subgroup
Rook Tuff, 802 ± 10 Ma [3]
Oodla Wirra Volc.
798 ± 5 Ma, 799 ± 3 Ma [4]
Wooltana Volcanics and equivalent
Arkaroola Subgroup
Callana Group
Warrina Supergroup
Mt Craford granite, 812 ± 6 Ma
Oakbank Inlier granite, 856 ±20 Ma[5]
GDS, 827 ± 6 Ma [6]
Archean to Mesoproterozoic basement
Legend
Tillite, glaciogenic sediments
siltstone, shale, slate
limestone, dolostone, marble
sandstone, quartzite, conglomerate
Basalt
Granite
Dated rock unit
Unconformity

Fig. 2

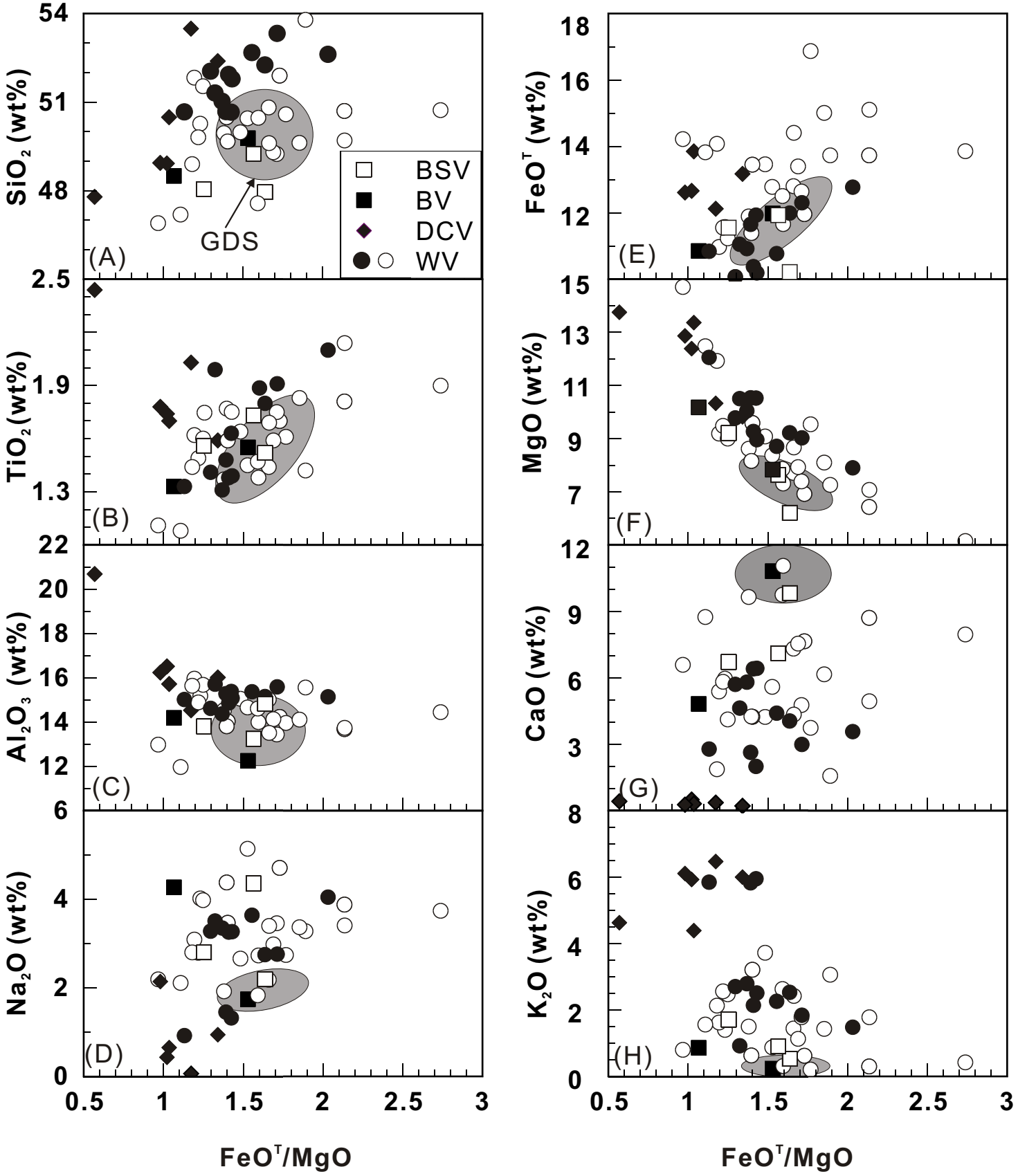
SiO2 (wt%)
TiO2 (wt%)
Al2O3 (wt%)
Na2O (wt%)
FeOT (wt%)
MgO (wt%)
CaO (wt%)
K2O (wt%)
FeOT/MgO
FeOT/MgO
(A)
(B)
(C)
(D)
(E)
(F)
(G)
(H)
GDS
BSV
BV
DCV
WV

Fig. 3

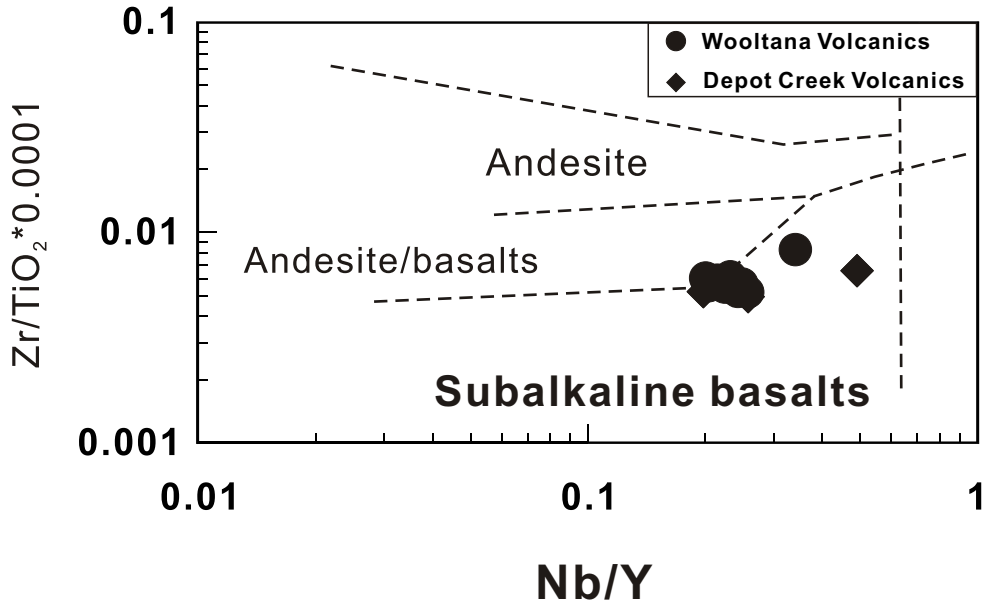
0.1
0.01
0.001
0.01
0.1
1
Zr/TiO2*0.0001
Nb/Y
Wooltana Volcanics
Depot Creek Volcanics
Andesite
Andesite/basalts
Subalkaline basalts

Fig. 4

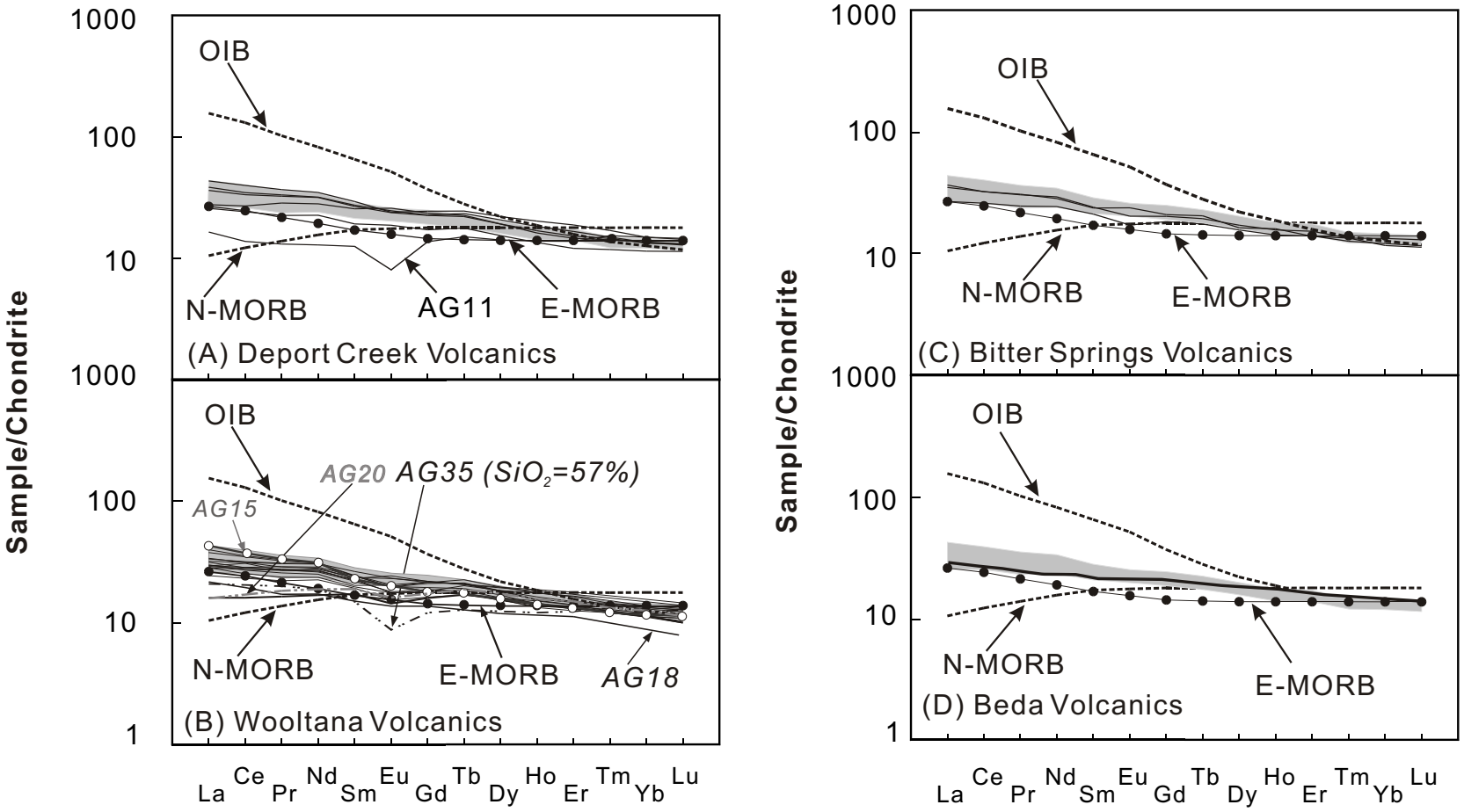
Sample/Chondrite
1000
100
10
1
OIB
N-MORB
AG11
E-MORB
(A) Deport Creek Volcanics
AG15
AG20
AG35 (SiO2=57%)
AG18
(B) Wooltana Volcanics
(C) Bitter Springs Volcanics
(D) Beda Volcanics
La Ce Pr Nd Sm Eu Gd Tb Dy Ho Er Tm Yb Lu

Fig. 5

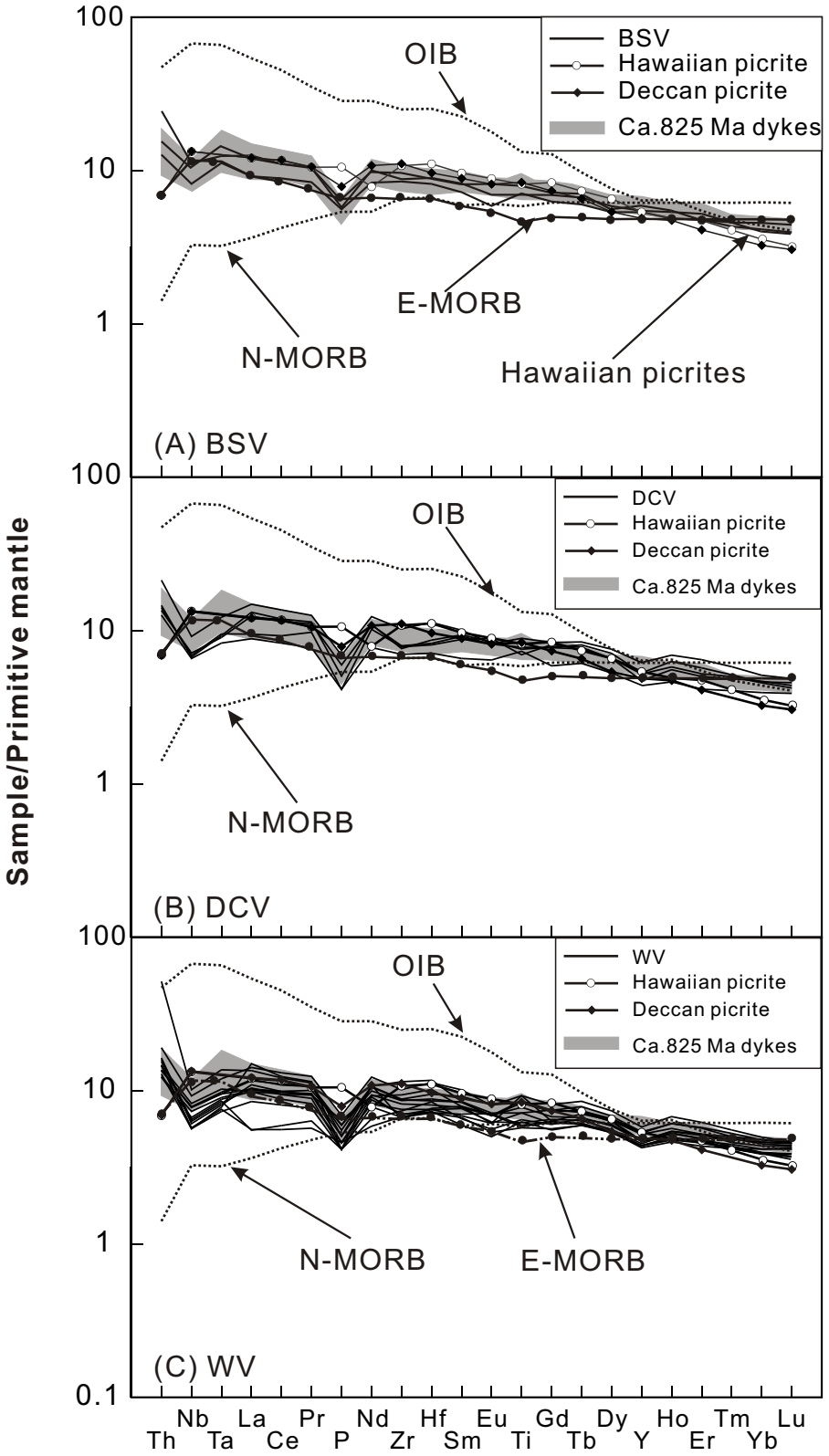
Sample/Primitive mantle
100
10
1
0.1
OIB
N-MORB
E-MORB
Hawaiian picrites
BSV
Hawaiian picrite
Deccan picrite
Ca.825 Ma dykes
(A) BSV
DCV
(B) DCV
WV
(C) WV
Th Nb Ta La Ce Pr P Nd Zr Hf Sm Eu Ti Gd Tb Dy Y Ho Er Tm Yb Lu

Fig. 6

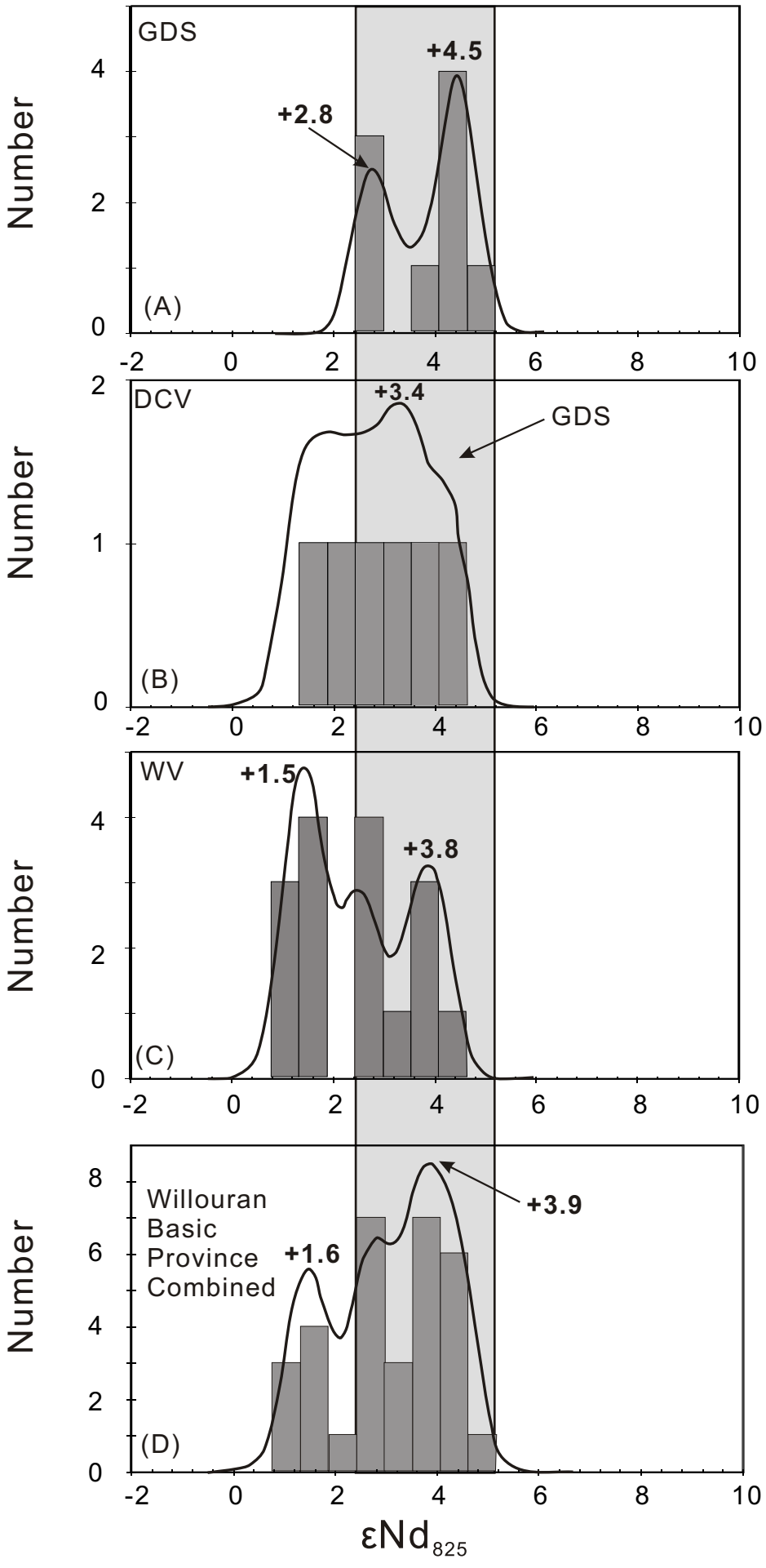
GDS
+4.5
+2.8
(A)
Number
DCV
+3.4
GDS
(B)
WV
+1.5
+3.8
(C)
Willouran
Basic
Province
Combined
+1.6
+3.9
(D)
εNd825

Fig. 7

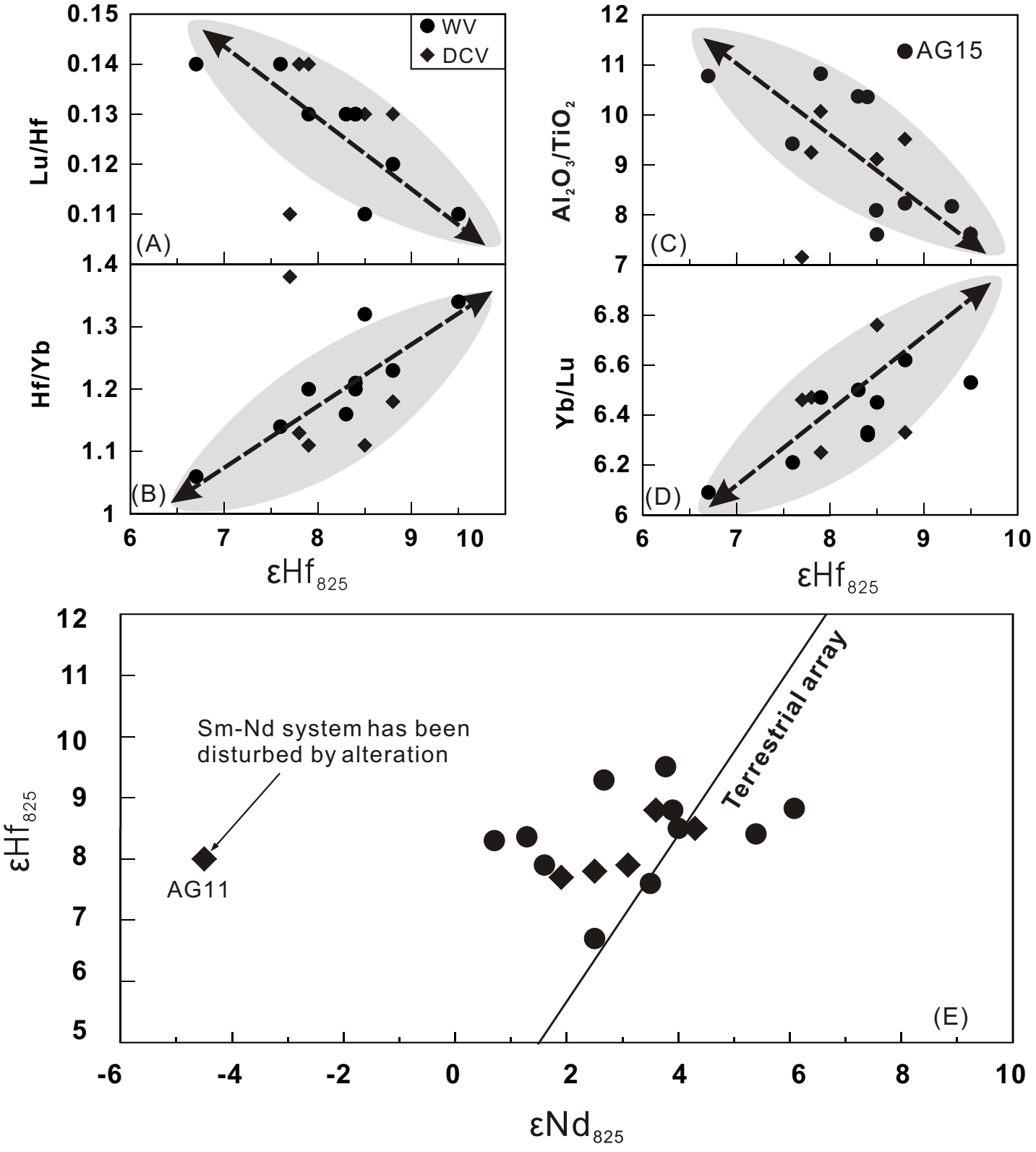
WV
DCV
AG15
Lu/Hf
Hf/Yb
Al_2O_3/TiO_2
Yb/Lu
(A)
(B)
(C)
(D)
(E)
εHf_{825}
εNd_{825}
Sm-Nd system has been disturbed by alteration
AG11
Terrestrial array

Fig. 8

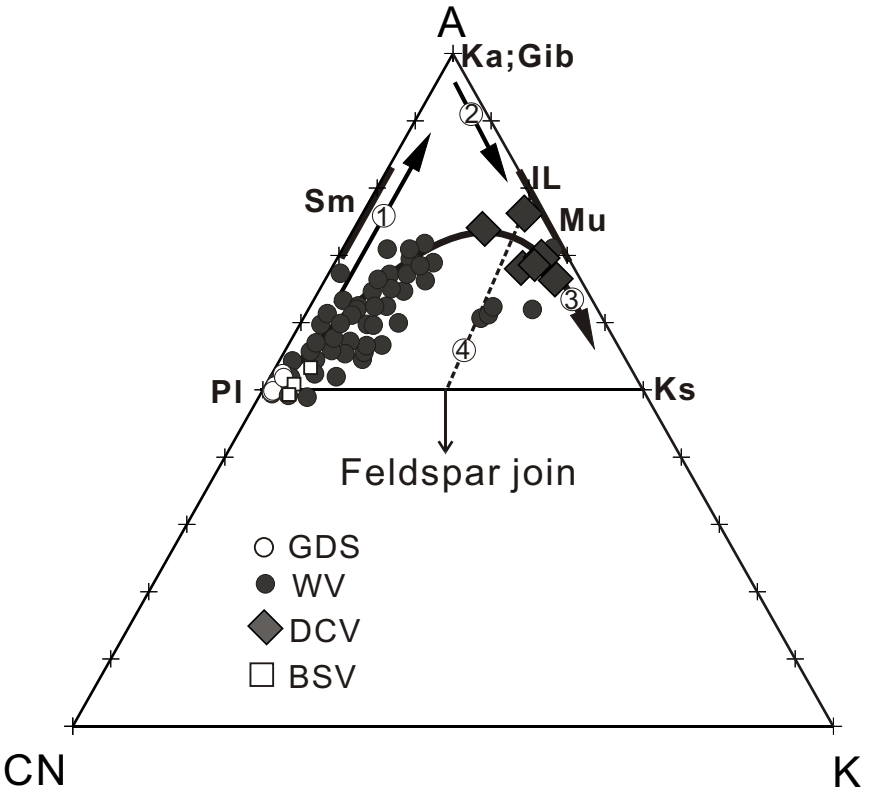

Fig. 9

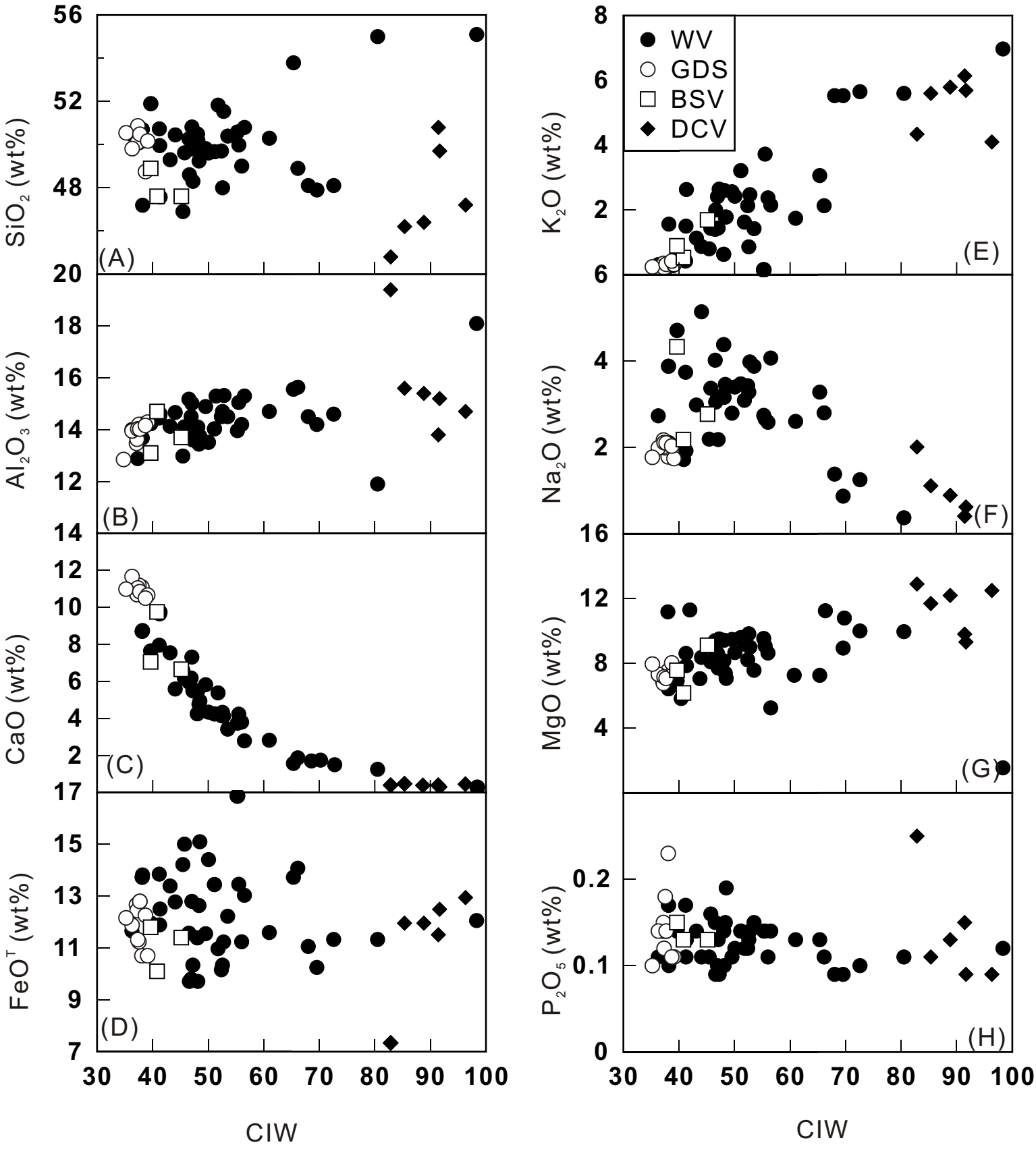
WV
GDS
BSV
DCV
SiO2 (wt%)
Al2O3 (wt%)
CaO (wt%)
FeOT (wt%)
K2O (wt%)
Na2O (wt%)
MgO (wt%)
P2O5 (wt%)
(A)
(B)
(C)
(D)
(E)
(F)
(G)
(H)
CIW
CIW

Fig. 10

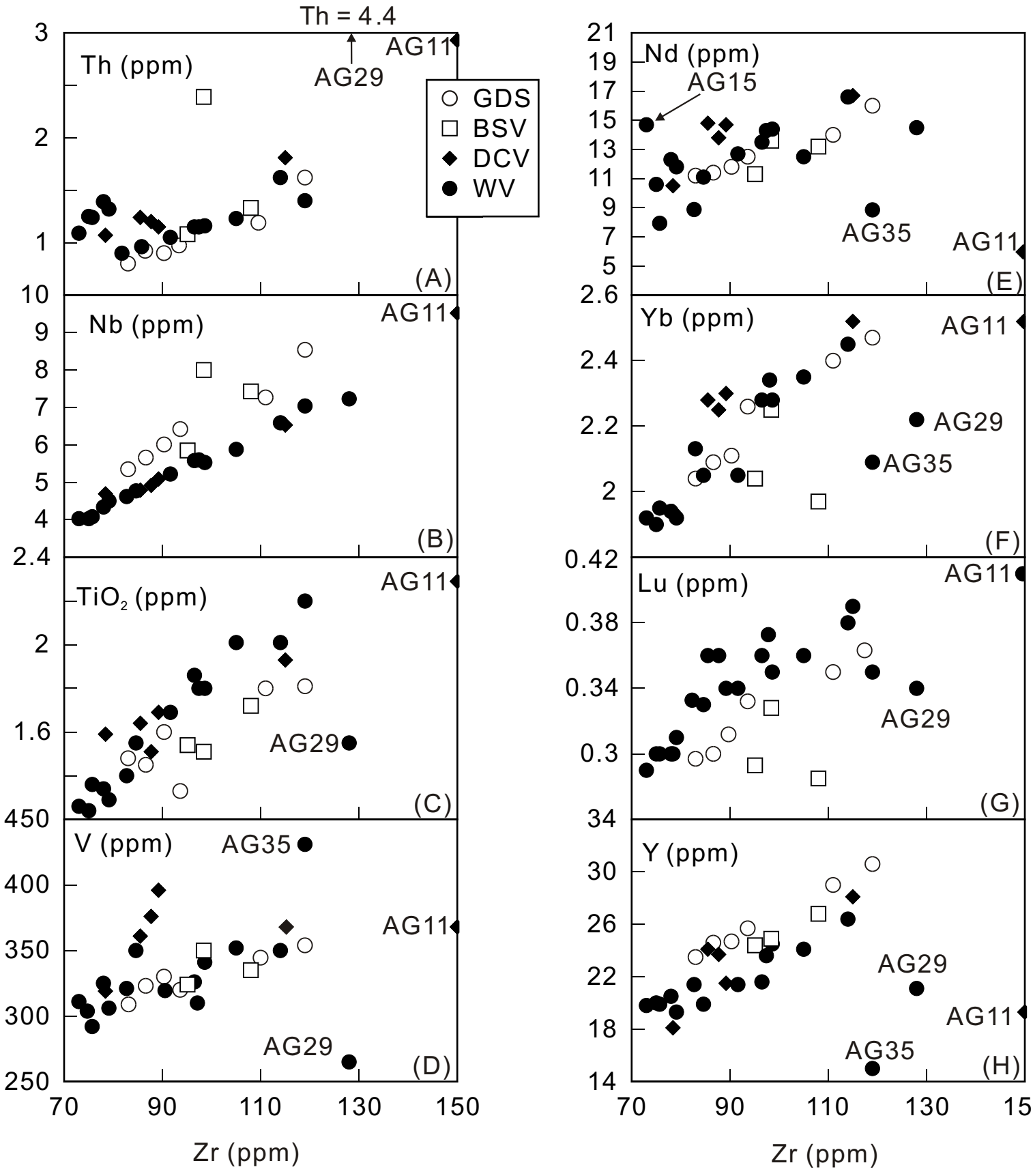
Th = 4.4
AG11
AG29
Th (ppm)
GDS
BSV
DCV
WV
(A)
AG11
Nb (ppm)
(B)
AG11
TiO2 (ppm)
AG29
(C)
V (ppm)
AG35
AG11
AG29
(D)
70
90
110
130
150
Zr (ppm)
Nd (ppm)
AG15
AG35
AG11
(E)
Yb (ppm)
AG11
AG29
AG35
(F)
Lu (ppm)
AG11
AG29
(G)
Y (ppm)
AG29
AG11
AG35
(H)
70
90
110
130
150
Zr (ppm)

Fig. 11

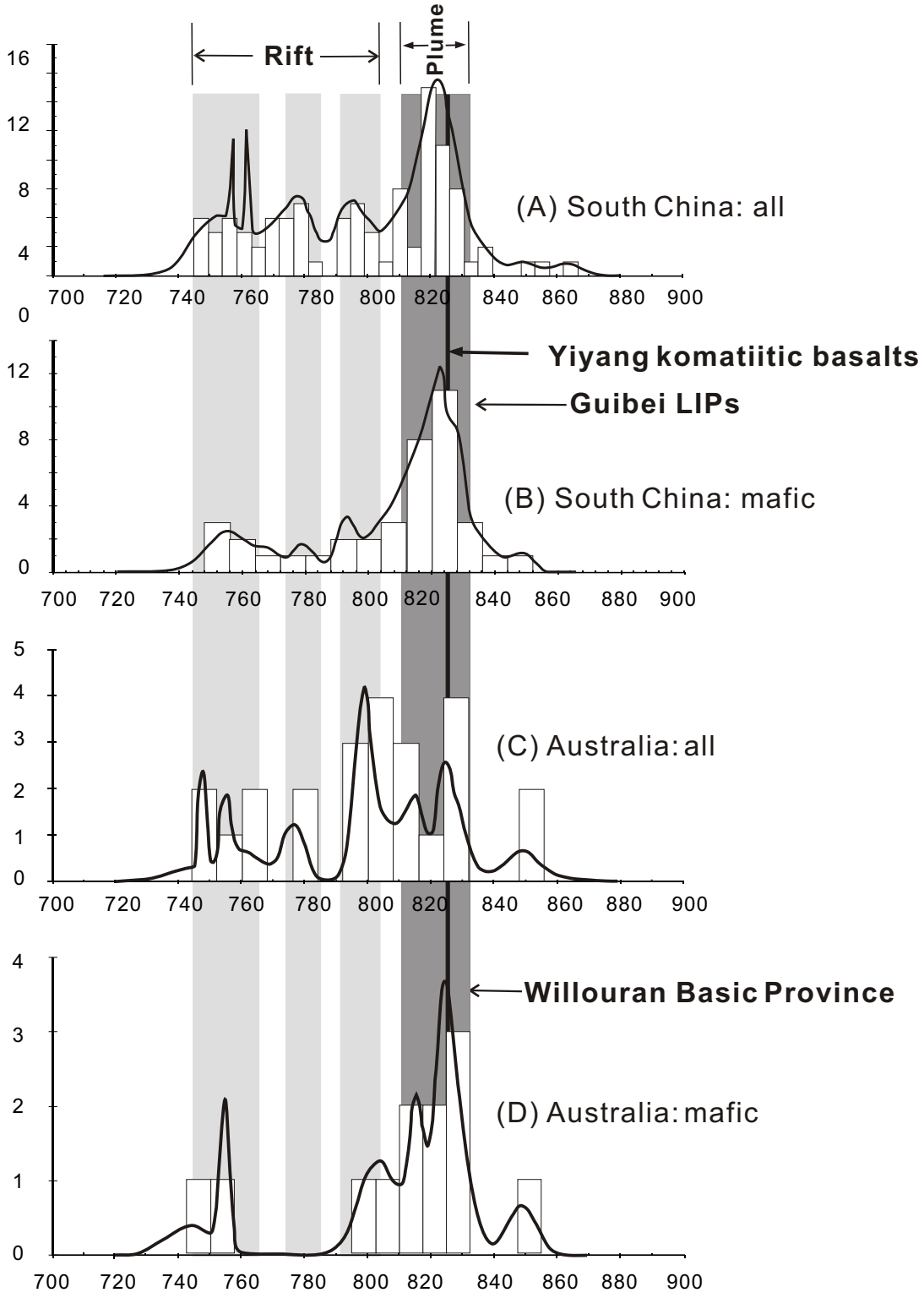

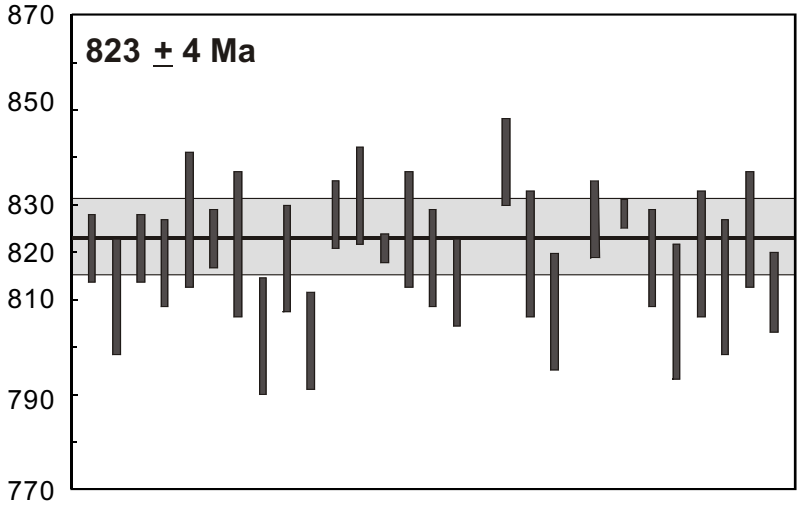

(E) Weighted mean age of the Guibei LIP, South China

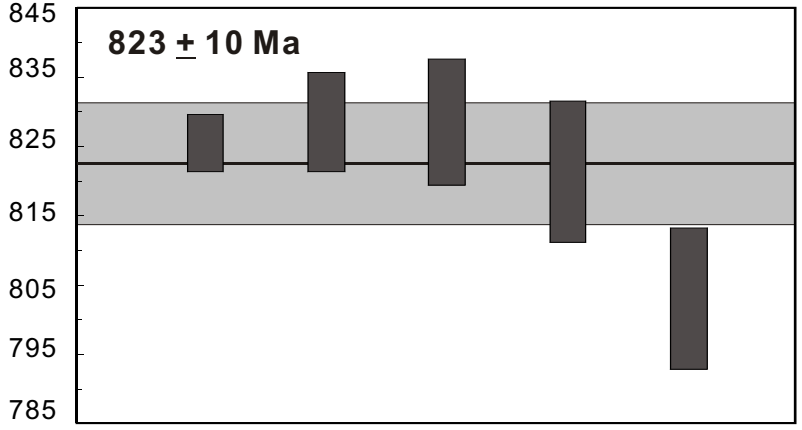

(F) Weighted mean age of the Willouran Basic Province, South Australia

Fig. 12

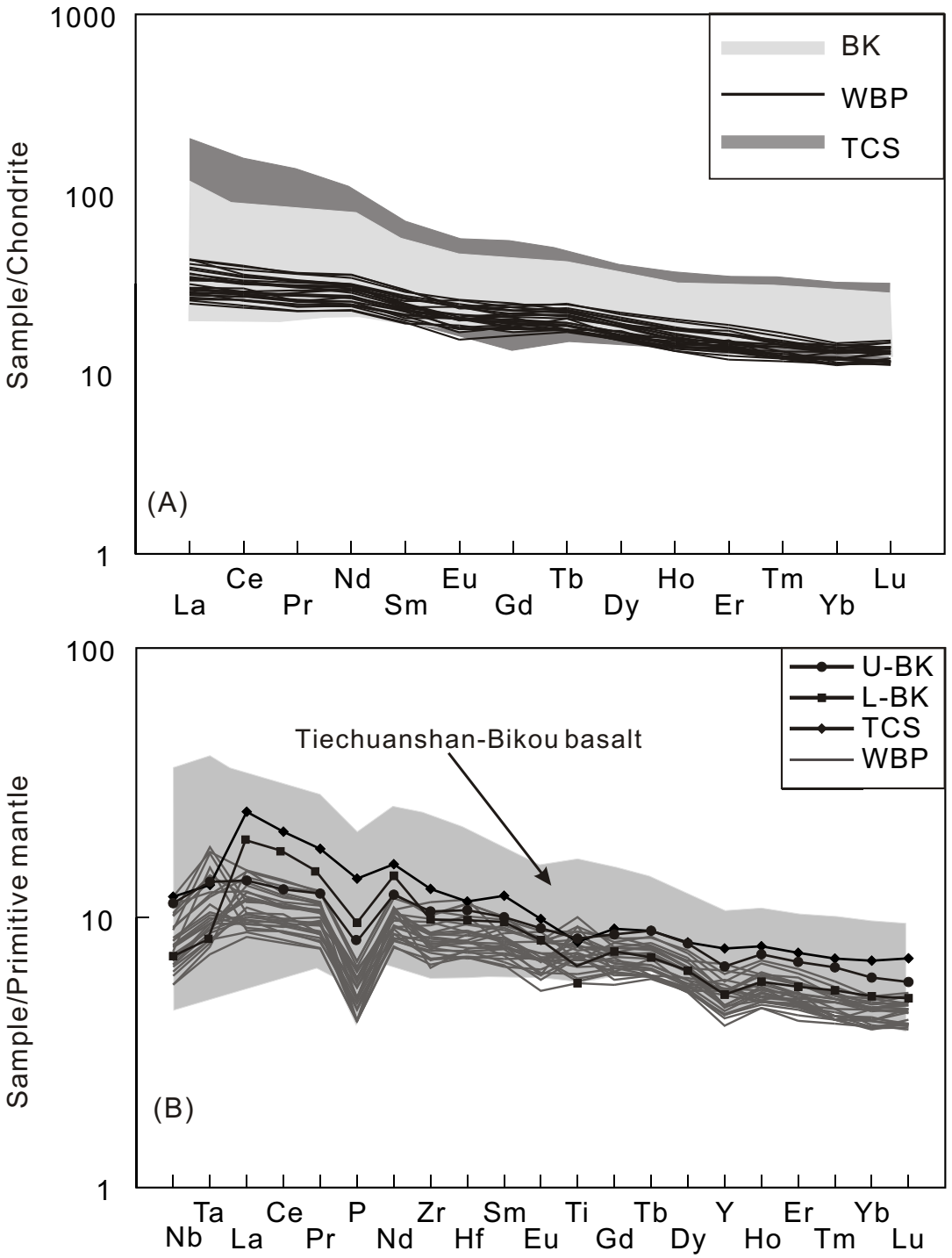
1000
100
10
1
Sample/Chondrite
BK
WBP
TCS
(A)
La
Ce
Pr
Nd
Sm
Eu
Gd
Tb
Dy
Ho
Er
Tm
Yb
Lu
100
10
1
Sample/Primitive mantle
U-BK
L-BK
TCS
WBP
Tiechuanshan-Bikou basalt
(B)
Nb
Ta
La
Ce
Pr
P
Nd
Zr
Hf
Sm
Eu
Ti
Gd
Tb
Dy
Y
Ho
Er
Tm
Yb
Lu

Fig. 13

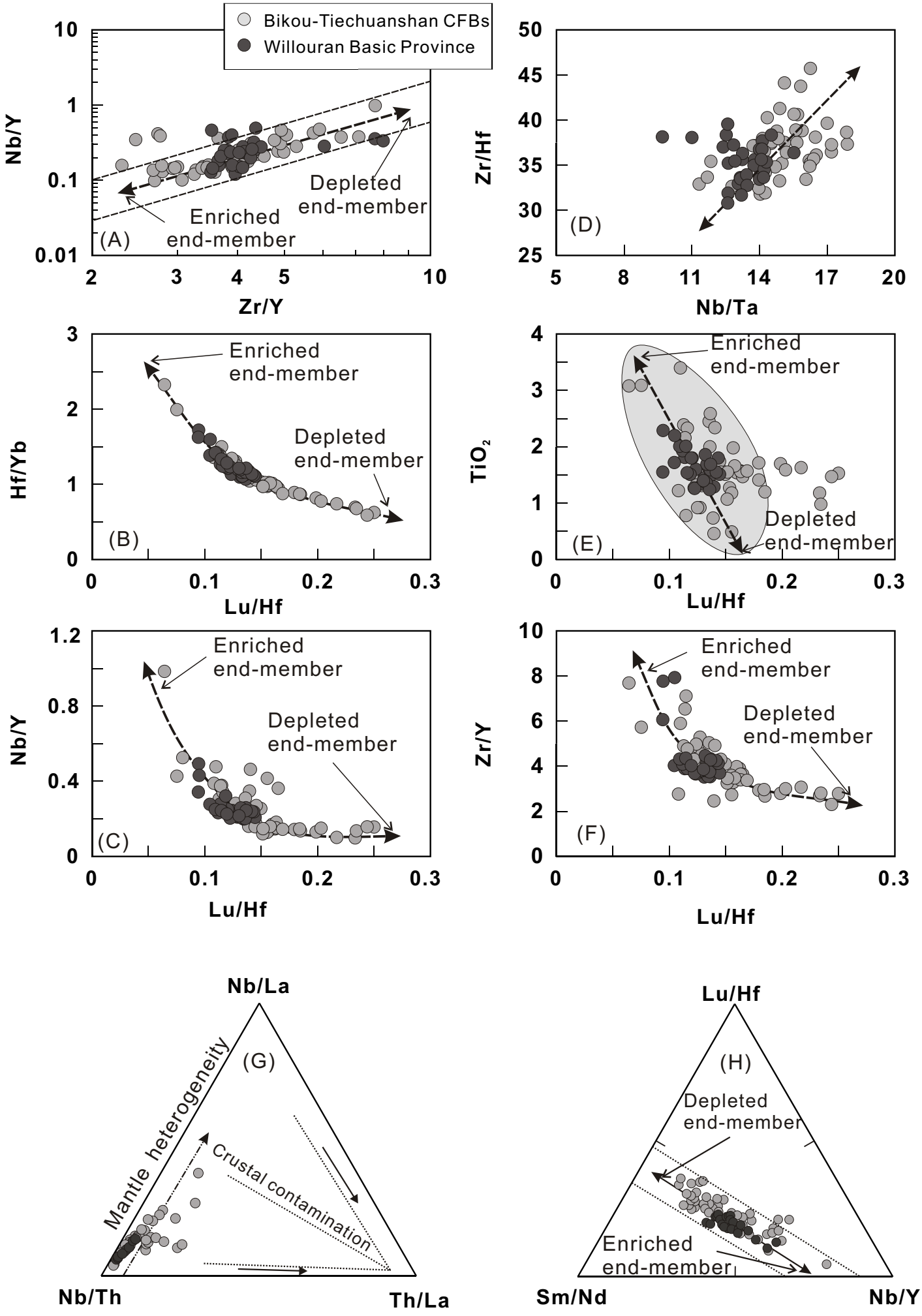
Bikou-Tiechuanshan CFBs
Willouran Basic Province
Nb/Y
Zr/Y
Enriched end-member
Depleted end-member
(A)
Zr/Hf
Nb/Ta
(D)
Hf/Yb
Lu/Hf
(B)
TiO2
(E)
(C)
Zr/Y
(F)
Nb/La
Nb/Th
Th/La
(G)
Mantle heterogeneity
Crustal contamination
Lu/Hf
Sm/Nd
Nb/Y
(H)

Fig. 14

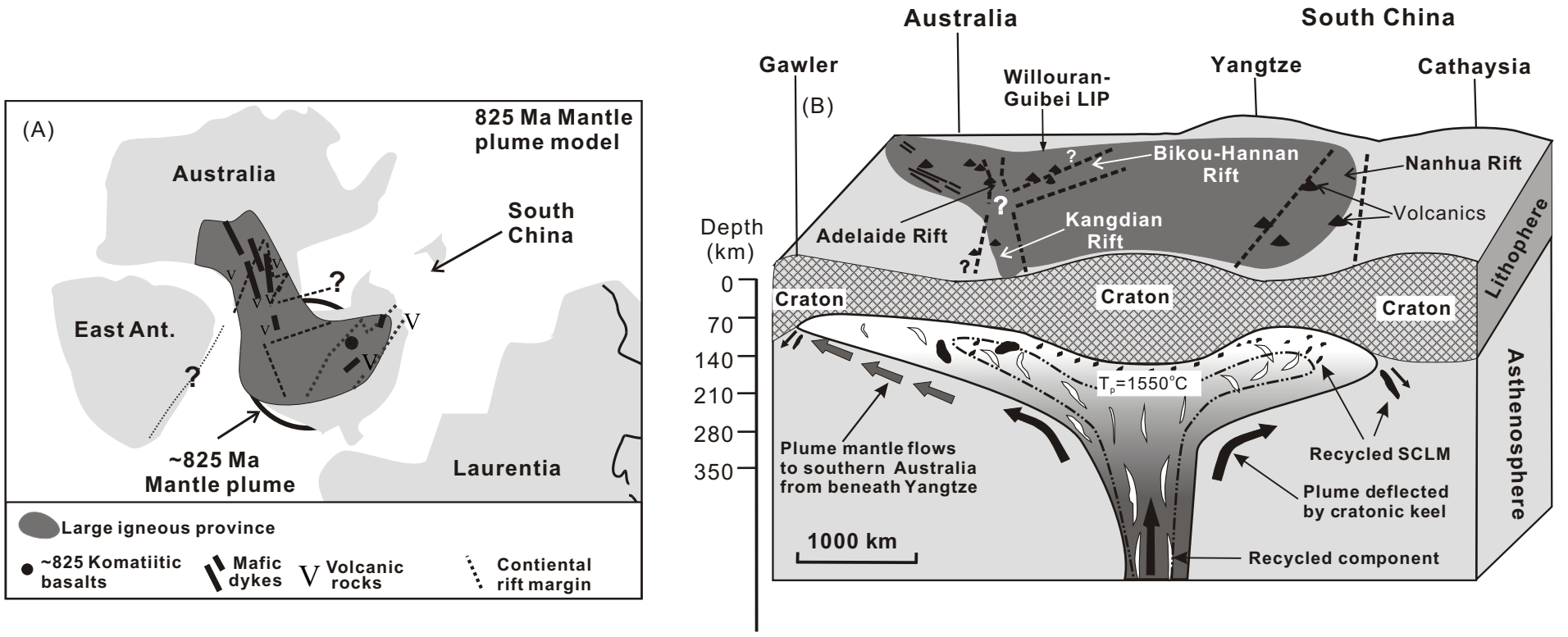
(A)
825 Ma Mantle plume model
Australia
South China
East Ant.
Laurentia
~825 Ma Mantle plume
Large igneous province
~825 Komatiitic basalts
Mafic dykes
Volcanic rocks
Contiental rift margin
(B)
Australia
South China
Gawler
Willouran-Guibei LIP
Yangtze
Cathaysia
Bikou-Hannan Rift
Nanhua Rift
Volcanics
Adelaide Rift
Kangdian Rift
Depth (km)
0
70
140
210
280
350
Craton
Craton
Craton
Lithophere
Asthenosphere
T_p=1550°C
Plume mantle flows to southern Australia from beneath Yangtze
Recycled SCLM
Plume deflected by cratonic keel
1000 km
Recycled component

Fig. 15